

Rate enhancement of gated drift-diffusion process by optimal resetting

Arup Biswas,¹ Arnab Pal,^{1, a)} Debasish Mondal,² and Somrita Ray^{2,3, b)}

¹⁾The Institute of Mathematical Sciences, CIT Campus, Taramani, Chennai 600113, India & Homi Bhabha National Institute, Training School Complex, Anushakti Nagar, Mumbai 400094, India

²⁾Department of Chemistry, Indian Institute of Technology Tirupati, Tirupati 517619, India

³⁾SUPA, School of Physics & Astronomy, University of Edinburgh, Peter Guthrie Tait Road, Edinburgh EH9 3FD, United Kingdom.

(Dated: 9 October 2023)

‘Gating’ is a widely observed phenomenon in biochemistry that describes the transition between the activated (or open) and deactivated (or closed) states of an ion-channel, which makes transport through that channel highly selective. In general, gating is a mechanism that imposes an additional restriction on a transport, as the process ends only when the ‘gate’ is open and continues otherwise. When diffusion occurs in presence of a constant bias to a *gated* target, i.e., to a target that switches between an open and a closed state, the dynamics essentially slows down compared to *ungated* drift-diffusion, resulting in an increase in the mean completion time, $\langle T^G \rangle > \langle T \rangle$, where T denotes the random time of transport and G indicates gating. In this work, we utilize stochastic resetting as an external protocol to counterbalance the delay due to gating. We consider a particle in the positive semi-infinite space that undergoes drift-diffusion in the presence of a stochastically gated target at the origin and is moreover subjected to a rate-limiting resetting dynamics. Calculating the minimal mean completion time $\langle T_{r^*}^G \rangle$ rendered by an optimal resetting rate r^* for this exactly-solvable system, we construct a phase diagram that owns three distinct phases: (i) where resetting can make gated drift-diffusion faster even compared to the original ungated process, $\langle T_{r^*}^G \rangle < \langle T \rangle < \langle T^G \rangle$, (ii) where resetting still expedites gated drift-diffusion, but not beyond the original ungated process, $\langle T \rangle \leq \langle T_{r^*}^G \rangle < \langle T^G \rangle$, and (iii) where resetting fails to expedite gated drift-diffusion, $\langle T \rangle < \langle T^G \rangle \leq \langle T_{r^*}^G \rangle$. We also highlight various non-trivial behaviors of the completion time as the resetting rate, gating parameters and the geometry of the set-up are carefully ramified. Gated drift-diffusion aptly models various stochastic processes such as chemical reactions that exclusively take place for certain activated state of the reactants. Our work predicts the conditions where stochastic resetting can act as a useful strategy to enhance the rate of such processes without compromising on their selectivity.

PACS numbers: 05.40.-a, 05.40.Jc

I. INTRODUCTION

‘Gating’ in biochemistry typically refers to the transition between the *open* and *closed* states of an ion channel; the ions are allowed to flow through the channel only when it is open¹. In a gated chemical reaction, the reactant molecules switch between a reactive and a non-reactive state; the collisions between the reactants *must* happen in their reactive states for a successful reaction. Thus, gating is a signature of a constrained reaction/transport, be it an enzyme finding the correct substrate or a protein finding the target site along a DNA strand or associating to a cleavage site on a peptide. Given their very generic nature, it is no wonder why gated processes showcase a myriad of applications spanning across fields from chemistry^{2–5}, physics^{6–12} to biology^{13–15}.

Since the seminal works of Szabo *et al*^{4,6,16}, gated processes have gained considerable attention across a wide panorama of applications such as 1D gated continuous-time and discrete-space random search process in confinement⁸, intermittent switching dynamics of a protein undertaking facilitated diffusion on a DNA strand¹⁷, 3D gated diffusive search process with different diffusivities⁹, gated active particles¹⁸, to name a few. Gopich and Szabo explored the possibil-

ity of multiple gated particles/targets in a model with intrinsic reversible binding¹¹. More on a mathematical side, Lawley and Keener established a connection between a radiative/reactive boundary and a gated boundary in diffusion controlled reactions¹⁹. There has been a renewed interest in the field emanating from the works by Mercado-Vásquez and Boyer on a 1D gated diffusive process on the infinite line²⁰, Scher and Reuveni on gated reactions on arbitrary networks including random walk models both in continuous²¹ and discrete time²² and Kumar *et al* on threshold crossing events of a gated process²³ and inference of first-passage times from the detection times of gated diffusive first-passage processes²⁴. In a similar vein, in this work, we delve deeper into a gated diffusive process and in particular, focus on to design principles to improve efficiency of a gated reaction [see Fig. (1)].

For a gated diffusive process to be complete, a certain condition that mimics the open-gate-scenario, imposed either on the diffusing entity or on the target that it diffuses to, needs to be fulfilled. This additional restriction imposed due to gating certainly makes the process more selective, which is essential for the associated biochemical system to function properly. The cost for this selectivity, however, reflects on the completion time, which makes a gated diffusive process essentially slower than the corresponding ungated one. However, nature has its own way to curtail such situation to allow effective reactions. For example, consider a chemical reaction such as in Fig. (1) where an unbinding or a resetting from a metastable state can lead to a facilitated reaction. The ef-

^{a)}Electronic mail: arnabpal@imsc.res.in

^{b)}Electronic mail: sray@ed.ac.uk

fects of such resetting events are proven to be crucial not only in such chemical reactions^{25,26}, but also in the backtracking of RNA polymerase²⁷ and disassociation kinetics of RhoA in the membrane²⁸. Motion of the reactants or the morphogens which get produced constantly from a certain place inside the cell before degrading in time (due to their finite lifetime) can also be interpreted as stochastically restarted processes²⁹. More on the physics side, it has been established in the pioneering work of Evans and Majumdar³⁰ that stochastic resetting can be utilized as a powerful strategy to expedite the completion time of a 1D diffusive search process. This remarkable result led to many fascinating works where it was shown that indeed this intermittent resetting strategy can benefit the search processes conducted by diffusion controlled^{31–40} and non-diffusive stochastic processes^{41–44} [see here⁴⁵ for an extensive review of the subject]. Single particle experiments using optical traps have also paved the way of our understanding of resetting modulated search processes^{46,47}. Albeit these advances, there has been a persistent void in the understanding of resetting induced gated processes until recently when resetting mechanism has been used to reduce the average completion time of a gated diffusive process in 1D^{48,49}.

While resetting is a useful strategy to benefit *diffusive* transport of ions/ molecules in unbounded phase space, the same can not be said for a *drift-diffusive* search process. There, resetting can be useful only if the rate of diffusive transport is higher compared to the rate of driven transport^{50,51,54,55}. However, if the drift supersedes the transport of molecules across the channel, resetting can only hinder the completion rendering a higher transit time. This crucial interplay can then be understood in terms of the so-called Péclet number, which is a ratio between the diffusion- and drift-dominated microscopic time-scales^{50,51}. In fact, the role of resetting can be quantified within a universal set-up of first-passage under restart which essentially teaches us that resetting will be always beneficial if the underlying process without resetting has a coefficient of variation (often known as the signal to noise ratio) – a statistical measure of dispersion in the random completion time, defined as the ratio of its standard deviation to its mean – greater than unity^{42,56,57}. These observations naturally set the stage to understand the role of resetting in a gated drift-diffusive search process which, to the best of our knowledge, has not been studied so far. In particular, the central objective of this work is to understand whether resetting can enhance the completion rate of a gated drift-diffusive search process and if so, under what conditions. Unraveling the intricate role of drift, diffusion and gating along with that of resetting will be at the heart of this study.

To illustrate the set-up of the present work, let us consider a diffusive transport process confined to the positive semi-infinite space in presence of a constant drift which is directed towards a target that randomly switches between an open and a closed state with constant rates. This is a general scenario mimicked by, e.g., a chemical reaction [see Fig. 1], where the collisions between reactants [CR_1 and R_2] lead to the formation of product only when at least one of the reactants is in an activated state [when R_2 exists as R_2^*] and not otherwise. Since resetting is an integral part of any consecutive chemical

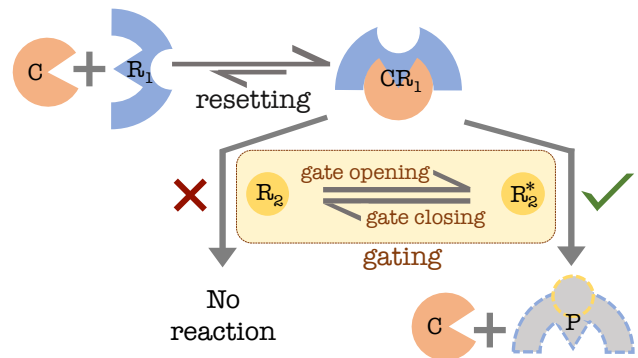


FIG. 1. Scheme for a gated chemical reaction between two reactants R_1 and R_2 , catalysed by C . In the first step, the catalyst initiates the reaction by binding reversibly with R_1 to generate CR_1 , a metastable intermediate: $C + R_1 \rightleftharpoons CR_1$. In the second step, CR_1 reacts selectively with R_2^* (the *reactive* or *open-gate* state of R_2) to generate the product P and liberate the catalyst: $CR_1 + R_2^* \rightarrow C + P$. This step can be modeled by gated drift-diffusion, while the unbinding of C from R_1 is essentially resetting.

reaction that has a reversible first-step [when C binds to, or unbinds from, R_1], the reaction scheme shown in Fig. 1 can be modeled as gated drift-diffusion with resetting. In this paper, we study the completion time statistics for this general set-up. In particular, we perform a comprehensive analysis to understand the role of optimal resetting in enhancing the rate of such transport and construct a complete phase diagram that distinguishes between the phases where (i) resetting accelerates gated drift-diffusion beyond the original (without resetting) ungated process, (ii) resetting still proves itself to be beneficial by improving the rate of gated drift-diffusion, but not beyond the original ungated process and (iii) resetting can not expedite gated drift-diffusion.

The rest of the paper is organized as follows. In Section II, we describe the model and follow a Fokker-Planck approach to write down the governing equations for gated drift-diffusion process that is subject to resetting. In the same Section, we solve those equations to calculate the mean completion time, denoted $\langle T_r^G \rangle$. We calculate the optimal resetting rate r^* that minimizes $\langle T_r^G \rangle$, and thereby investigate the conditions for resetting to expedite the process completion in Section III. There, various limits of the system parameters are also examined in detail. We calculate the maximal speedup that can be achieved, within our set-up, by the optimal resetting rate in Section IV. In Section V, we construct a full phase diagram that characterizes all the possible regimes underpinning the role of resetting in the process completion. We conclude with a brief summary and outlook of our work in Section VI. Some of the detailed derivations have been moved to the Appendix for brevity.

II. COMPLETION TIME STATISTICS

We start by casting the problem of gated chemical reaction [$CR_1 + R_2^* \rightarrow C + P$, introduced in Fig. 1] as gated drift-

diffusion. A convenient way to do so is to map the reaction coordinate associated to the reactants $CR_1 + R_2^*$ onto the starting position [$x_0 > 0$, see Fig. 2] of a particle that undergoes Brownian motion. Similarly, the reaction coordinate for the products $C + P$ can be mapped onto the position of a target [placed at the origin, see Fig. 2]. The chemical potential drive, which governs the reaction to its completion, can then be translated to a constant bias λ that the particle experiences while it diffuses to the target with a diffusion coefficient D . Note that λ is considered to be positive when it acts towards the target and negative when it acts away from the target. Such effective one-dimensional projection of the energy landscape of an enzyme or protein conformation is a well-adapted approach in the literature – see^{58–60} for more details. Nonetheless, there are a few key assumptions that we make during the mapping. First, we take into account an well-established fact that the chemical master equations for the discrete states can be coarse-grained into the Fokker-Planck equations for the reaction coordinates in the continuous space using a system size expansion^{61,62}. However, this conversion generically renders the drift and diffusion terms to be spatially dependent. In other words, the reaction coordinate associated to the catalysis process $CR_1 + R_2^* \rightarrow C + P$ is expected to diffuse in an *arbitrary* energy landscape, where the product state $C + P$ is usually denoted by the global minimum. However, to simplify the problem, we replace the general potential by a linear one, which leads to a constant drift velocity λ towards (or away from) the gated target. This is the second assumption that lies behind our analysis. Albeit these simplified approximations, the major advantage here is the elegant analytical tractability of the model from which one can also unveil the crucial interplay between the gated boundary and resetting/unbinding mechanism.

To model gating, the target is considered to randomly switch between a reactive ($\sigma = 1$ state in Fig. 2 that resembles R_2^* in Fig. 1) and a non-reactive state [$\sigma = 0$ state in Fig. 2 that resembles R_2 in Fig. 1]. The conversion from the non-reactive to the reactive state happens with a constant rate $\alpha > 0$ and that from the reactive to the non-reactive state happens with a constant rate $\beta > 0$ [Fig. 2]. Therefore, the *reactive occupancy* of the target, i.e., the probability of finding the target in its reactive state is $p_r := \alpha/(\alpha + \beta)$. Similarly, the *non-reactive occupancy* or the probability that the target is in its non-reactive state is $p_{nr} := (1 - p_r) = \beta/(\alpha + \beta)$. In analogy to the chemical reaction, the process ends only when the particle hits the target in its reactive state. When it hits the target in its non-reactive state, it simply gets reflected and continues to diffuse.

As mentioned in the Introduction, the unbinding of the catalyst C from R_1 can be interpreted as resetting at x_0 . For simplicity, here we consider Poissonian resetting with a constant rate r . In the gated drift-diffusion scenario, this means that the particle is taken back to x_0 after stochastic intervals of time, taken from an exponential waiting time distribution with mean r^{-1} . Note that here we assume that the resetting is instantaneous and once the particle is reset at x_0 , it immediately starts moving again. In other words, we neglect any refractory period, i.e., idle time after each resetting event be-

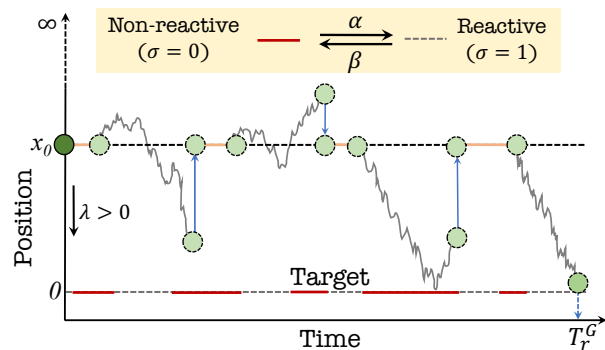


FIG. 2. Schematic diagram of a gated drift-diffusion process in semi-infinite space with resetting, where the target (placed at the origin) switches stochastically between a reactive state ($\sigma = 1$) and a non-reactive state ($\sigma = 0$). The transition from the non-reactive to the reactive state takes place with a constant rate $\alpha > 0$, and the opposite transition takes place with a constant rate $\beta > 0$. When the particle, starting at x_0 , hits the target in its reactive state (dashed line), the process ends. T_r^G marks the random completion time of the gated drift-diffusion process with resetting.

fore drift-diffusion resumes, considering that the time-scale of waiting at x_0 after reset [which maps to the time required for C to bind R_1 in Fig. 1] is much smaller compared to that of either drift-diffusion or resetting. We also assume that the intermittent dynamics of the target are independent of resetting similar to⁴⁸.

The fundamental quantity of interest here is the random completion time of the gated chemical reaction, i.e., the *first-passage time*⁶³ of the diffusing particle from x_0 to the target placed at the origin. To calculate the mean first-passage time (MFPT), we first need to write the backward Fokker-Planck equation for the survival probability of this system, which is the total probability to find the particle in the interval $[0, \infty)$ at a time t , provided the initial position is x_0 . We denote $Q_\sigma(t|x_0)$ as the joint survival probability, i.e., the probability that the particle has not been absorbed by the target up to time t , given the initial position x_0 and initial target state $\sigma(t=0)$. One can then construct the backward Fokker-Planck equations⁴⁸ in terms of the initial position x_0 , which now serves as a variable

$$\begin{aligned} \frac{\partial Q_0(t|x_0)}{\partial t} &= -\lambda \frac{\partial Q_0(t|x_0)}{\partial x_0} + D \frac{\partial^2 Q_0(t|x_0)}{\partial x_0^2} + \alpha [Q_1(t|x_0) \\ &\quad - Q_0(t|x_0)] + r [Q_0(t|x_r) - Q_0(t|x_0)], \\ \frac{\partial Q_1(t|x_0)}{\partial t} &= -\lambda \frac{\partial Q_1(t|x_0)}{\partial x_0} + D \frac{\partial^2 Q_1(t|x_0)}{\partial x_0^2} + \beta [Q_0(t|x_0) \\ &\quad - Q_1(t|x_0)] + r [Q_1(t|x_r) - Q_1(t|x_0)]. \end{aligned} \quad (1)$$

Note that x_r in the above set of equations indicates the resetting position which has to be distinguished from the variable x_0 initially and only at the end, has to be set $x_r = x_0$ self-consistently. The initial conditions for Eq. (1) are $Q_\sigma(0|x_0) = 1$ and the boundary conditions are $Q_1(t|0) = 0$ and $[\partial Q_0(t|x_0)/\partial x_0]_{x_0=0} = 0$, respectively. This indicates that the particle is absorbed at the target when the latter is reactive

($\sigma = 1$) and is reflected from the target when it is non-reactive ($\sigma = 0$)⁴⁸. The *average* survival probability for the gated process can then be written by taking contributions from both the possibilities

$$Q_r^G(t|x_0) = p_r Q_1(t|x_0) + (1 - p_r)Q_0(t|x_0). \quad (2)$$

Subsequently, we use subscript r and superscript G to indicate resetting and gating respectively in Eq. (2) and rest of the paper. The Laplace transformation of Eq. (2) gives

$$\tilde{Q}_r^G(s|x_0) = p_r \tilde{Q}_1(s|x_0) + (1 - p_r)\tilde{Q}_0(s|x_0), \quad (3)$$

where $\tilde{Q}_r^G(s|x_0) := \int_0^\infty dt e^{-st} Q_r^G(t|x_0)$ is the Laplace transform of $Q_r^G(t|x_0)$ and $\tilde{Q}_\sigma(s|x_0) := \int_0^\infty dt e^{-st} Q_\sigma(t|x_0)$ are Laplace transforms of $Q_\sigma(t|y)$, respectively. The average MFPT, our observable of interest in this work, is also defined over the two random possibilities and thus reads

$$\langle T_r^G(x_0) \rangle = p_r \langle T_1(x_0) \rangle + (1 - p_r) \langle T_0(x_0) \rangle, \quad (4)$$

where $\langle T_\sigma(x_0) \rangle$ is the MFPT when the initial state of the target is σ , given by $\langle T_\sigma(x_0) \rangle = \int_0^\infty dt Q_\sigma(t|x_0) = \tilde{Q}_\sigma(s|x_0)|_{s=0}$, since $-\partial Q_\sigma(t|x_0)/\partial t$ is the associated first-passage time distribution^{62,63}. Therefore, the average MFPT reads

$$\langle T_r^G(x_0) \rangle = \int_0^\infty dt Q_r^G(t|x_0) = \tilde{Q}_r^G(s|x_0)|_{s=0}. \quad (5)$$

For the rest of the paper, we will write $\langle T_r^G \rangle$ instead of $\langle T_r^G(x_0) \rangle$ for brevity.

Solving Eq. (1) in the Laplace space, plugging in the solutions, i.e., $\tilde{Q}_\sigma(s|x_0)$ s, into Eq. (3) to calculate $\tilde{Q}_r^G(s|x_0)$ and finally setting $s = 0$ in the resulting expression of $\tilde{Q}_r^G(s|x_0)$ following Eq. (5), we obtain [see Appendix A for detailed derivation] the explicit expression of the average MFPT that reads

$$\langle T_r^G \rangle = \frac{1}{r} (e^{\mu_1 x_0} - 1) + \frac{\beta \mu_1}{\alpha \mu_2} \left(\frac{1}{r} + \frac{e^{-\mu_2 x_0}}{\alpha + \beta} \right) e^{\mu_1 x_0}, \quad (6)$$

where $\mu_1 = (-\lambda + \sqrt{\lambda^2 + 4Dr})/2D > 0$ and $\mu_2 = (-\lambda + \sqrt{\lambda^2 + 4D(\alpha + \beta + r)})/2D > 0$. Therefore, for pure diffusion with gating, i.e., when $\lambda \rightarrow 0$, $\mu_1 = \sqrt{r/D}$ and $\mu_2 = \sqrt{(r + \alpha + \beta)/D}$ and Eq. (6) boils down to⁴⁸

$$\langle T_r^G \rangle = \frac{e^{\sqrt{\frac{r}{D}} x_0} - 1}{r} + \frac{\beta e^{\sqrt{\frac{r}{D}} x_0}}{\alpha \sqrt{r[r + \alpha + \beta]}} \left[1 + \frac{r e^{-\sqrt{\frac{r + \alpha + \beta}{D}} x_0}}{(\alpha + \beta)} \right]. \quad (7)$$

Moreover, in the absence of gating, i.e., when $\beta \rightarrow 0$, Eq. (6) reduces to $\langle T_r \rangle = [\exp(x_0(\sqrt{\lambda^2 + 4Dr} - \lambda)/2D) - 1]/r$, which is the exact expression for the MFPT for ungated drift-diffusion with Poissonian resetting⁵⁰.

In Fig. 3, we plot $\langle T_r^G \rangle$ as a function of the resetting rate r for different values of the drift velocity λ , where the reactive occupancy of the target, p_r , is kept constant. It is evident from Fig. 3 that when $\lambda > 0$, i.e., when the drift acts towards the target, the average MFPT shows a non-monotonic variation with

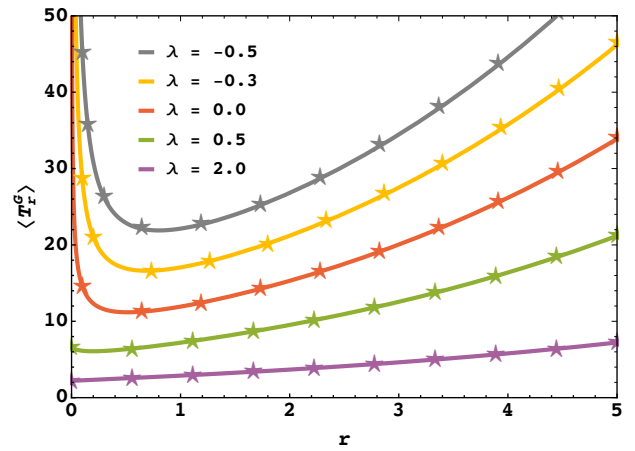


FIG. 3. The average MFPT, $\langle T_r^G \rangle$, vs the resetting rate r for different values of the drift velocity λ . The lines represent analytical results following Eq. (6) and the symbols represent results from numerical simulations [see Appendix D for details]. The curves with $\lambda > 0$ denote cases where the drift acts towards the gated target and that with $\lambda < 0$ denote otherwise. The variation of $\langle T_r^G \rangle$ with r is always non-monotonic for $\lambda \leq 0$, however, for $\lambda > 0$ it is non-monotonic for lower values of λ , but monotonic for sufficiently high values of λ . Here we take $x_0 = 2$, $D = 1$, $\alpha = 0.5$, and $\beta = 0.5$ for all cases.

r for lower values of λ , indicating that the introduction of resetting expedites first-passage when the process is diffusion-controlled. In contrast, $\langle T_r^G \rangle$ increases monotonically with r for sufficiently higher values of λ , meaning that the introduction of resetting delays first-passage when the process is drift-controlled. This trend can be explained in the following way. When diffusion dominates over the drift, the particle tends to diffuse away from the target. In such cases, resetting can effectively truncate those long trajectories, which reduces the overall first-passage time. In contrast, when the drift dominates over diffusion, the particle tends to execute a directed motion towards the target ($\lambda > 0$); resetting can only hinder such transport resulting in a longer completion time. Note that resetting can accelerate first-passage even when the dynamics is drift-controlled, if the drive is away from the target ($\lambda < 0$).

Summarizing, we see that either for pure diffusion or when the drift acts away from the target ($\lambda \leq 0$), the average MFPT consistently shows a non-monotonic variation with r . This means that the introduction of resetting always accelerates first-passage for $\lambda \leq 0$. Thus, a hallmark of *resetting transition* is apparent for $\lambda > 0$, while no such transition is expected for $\lambda \leq 0$. Indeed, similar to ungated diffusive processes under resetting^{30,31}, introduction of resetting was shown to be always beneficial for pure diffusive gated process ($\lambda = 0$) and no such transition was observed there⁴⁸. Here, we focus on the scenario when the drift acts towards the target and then reveal the physical conditions under which resetting strategy turns out to be beneficial. In passing, we will also briefly discuss a situation where the system is confined between two boundaries (one additional reflecting boundary apart from the stochastically gated target). In analogy to a chemical reaction, the reflecting boundary is often used to mimic high activa-

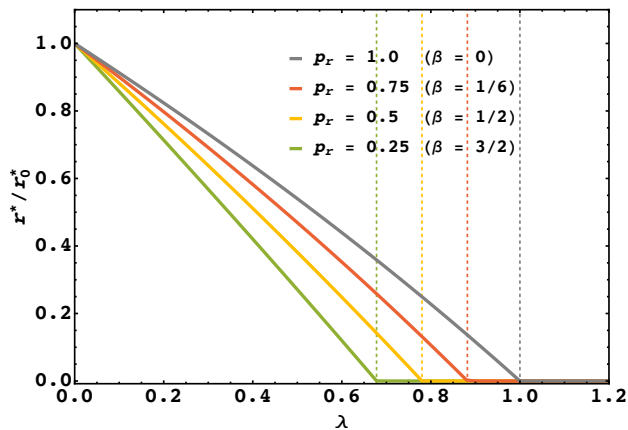


FIG. 4. The scaled optimal resetting rate, r^*/r_0^* , vs λ for different values of p_r . Resetting transition in each case is observed at $\lambda = \lambda_c$, where the scaled ORR becomes zero, marked by dashed lines of the same color as the curve. For $\lambda < \lambda_c$, resetting expedites transport, whereas for $\lambda \geq \lambda_c$ it can not. Here we take $D = 1$, $x_0 = 2$, and $\alpha = 0.5$ [which leads to $p_r = 1/(2\beta + 1)$] for all cases. For ungated drift-diffusion [given by $p_r = 1$, since $\beta \rightarrow 0$], the resetting transition is observed at $\lambda_c = 1$ (gray curve). For gated drift-diffusion with $p_r < 1$, λ_c decreases below unity.

tion energy barriers in reaction coordinate. We refer to Appendix B for this discussion, where we investigate the role of resetting in details.

III. THE OPTIMAL RESETTING RATE AND A PHASE DIAGRAM FOR EXPEDITED COMPLETION

The resetting transition is traditionally captured by the optimal resetting rate (ORR, denoted r^*), defined as the rate of resetting that minimizes the average MFPT. Fig. 3 reveals that for pure diffusion ($\lambda = 0$) the optimal resetting rate has a certain positive value (denoted $r^* = r_0^*$, not marked in Fig. 3). With increase in the drift towards the target, ORR gradually decreases to finally become zero at a critical value of λ (denoted λ_c , not shown in Fig. 3), which marks the point of resetting transition. If we continue to increase λ beyond λ_c , ORR remains zero. Note that when the drift acts away from the target ($\lambda < 0$), r^* increases as that drift becomes stronger. The optimal resetting rate r^* thus acts as an order parameter, in the similar spirit as in classical phase transition, to explore the resetting transition. Since ORR minimizes $\langle T_r^G \rangle$, it can be calculated from the relation $d\langle T_r^G \rangle/dr|_{r=r^*} = 0$, which leads to a complicated transcendental equation that can not be solved analytically. Solving the same numerically, we calculate r^* , the optimal resetting rate for $\lambda > 0$. In a similar manner, the optimal resetting rate for pure diffusion (for $\lambda = 0$, denoted r_0^*) is also obtained in order to calculate the scaled ORR, r^*/r_0^* .

In Fig. 4, we plot the scaled ORR with respect to λ for different values of the reactive occupancy p_r (we keep α constant and tune p_r by solely changing β). The non-zero values

of the scaled ORR for $\lambda < \lambda_c$ in Fig. 4 shows that resetting accelerates first-passage in that regime. In stark contrast, for $\lambda \geq \lambda_c$ the scaled ORR is zero, which shows that resetting can not accelerate first-passage in that regime. For the ungated ($p_r = 1$) process, $\lambda_c = 1$ for our choice of parameters, which is in exact agreement with earlier literature⁵⁰. It is evident from Fig. 4 that λ_c decreases when p_r is decreased below unity, which means that resetting expedites first-passage time upto a critical drift (which is essentially smaller than λ_c for the ungated process) when gating is introduced to the system.

In order to better understand how the critical value of λ changes with the reactive occupancy of the target, next we numerically calculate λ_c as a function of p_r . In Fig. 5, we construct a phase diagram spanned by the reactive occupancy p_r and the drift velocity λ , where λ_c acts as the separatrix that divides the entire phase space in two parts; one where resetting expedites first-passage (white regime) and the other where it can not (gray regime). We can recover the core results observed in Fig. 4 from Fig. 5 in the following way. For each value of $p_r \in [0, 1]$ [encountered by moving horizontally through Fig. 5], the dynamics is diffusion-controlled and resetting is beneficial if $\lambda < \lambda_c$, whereas the dynamics is drift-controlled and resetting turns out to be non-beneficial if $\lambda \geq \lambda_c$. It is clear from Fig. 5 as well that with increase in reactive occupancy, λ_c increases to finally become unity for the ungated process ($p_r = 1$). Fig. 5 is, therefore, a complete yet compact representation of the condition for resetting to expedite gated drift-diffusion. Next, we discuss an alternative approach that can successfully generate this phase diagram by

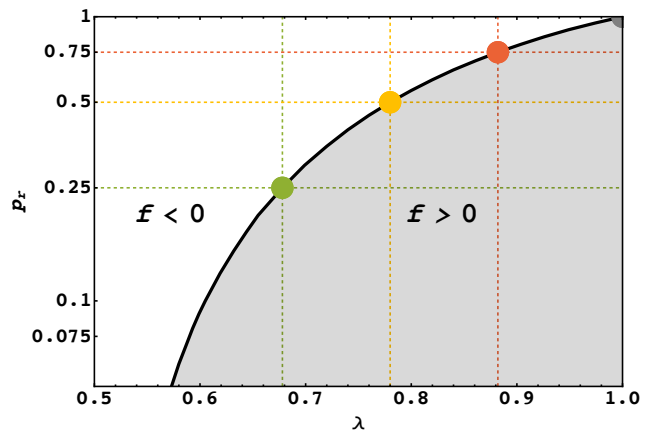


FIG. 5. A phase diagram of p_r vs. λ based on the qualitative effect of resetting on gated drift-diffusion. The black line represents the condition for resetting transition (λ_c), which divides the entire phase space in two parts. For $\lambda < \lambda_c$ resetting expedites transport (white regime), whereas for $\lambda \geq \lambda_c$ resetting fails to expedite transport (gray regime). Here we take $D = 1$, $x_0 = 2$ and $\alpha = 0.5$ [i.e., $p_r = 1/(2\beta + 1)$] for all cases. For the ungated process ($p_r = 1$), $\lambda_c = 1$ and it decreases with p_r . The colored discs on the black line present the cases shown in Fig. 4. Following the analysis of $\langle T_r^G \rangle$ in the limit $r \rightarrow 0$ [see Eq. (8) and Eq. (10)], the separatrix (black line) is also obtained by plotting $f = 0$. Resetting is beneficial for $f < 0$ (white regime), but not for $f > 0$ (gray regime).

carefully exploring the resetting criterion in the limit $r \rightarrow 0$.

Revisiting Fig. 3, we see that it clearly indicates when initial (in the limit $r \rightarrow 0$) slope of the $\langle T_r^G \rangle$ vs. r curve is negative, introduction of resetting proves itself beneficial by decreasing the average MFPT. In contrast, a positive slope of such curve in the limit $r \rightarrow 0$ suggests that introduction of resetting increases the average MFPT there. This motivates us to explore the condition for resetting to accelerate gated drift-diffusion by analyzing the expression of the average MFPT in the limit $r \rightarrow 0$. To do that, we first expand $\langle T_r^G \rangle$ in r for an infinitesimal resetting rate to obtain

$$\langle T_r^G \rangle \approx \langle T^G \rangle + r \left[\frac{\partial \langle T_r^G \rangle}{\partial r} \right]_{r=0} + O(r^2), \quad (8)$$

where $\langle T^G \rangle$ is the average MFPT in the absence of resetting. Following Eq. (6), we get [see Appendix C for an alternative derivation]

$$\langle T^G \rangle = \frac{1}{\lambda} \left[x_0 + \frac{2\beta D}{\alpha \left(\sqrt{4\alpha D + 4\beta D + \lambda^2} - \lambda \right)} \right]. \quad (9)$$

Note that in the absence of gating ($p_r = 1$, or $\beta = 0$), Eq. (9) reduces to $\langle T \rangle = x_0/\lambda$ ⁶³, which implies that $\langle T^G \rangle > \langle T \rangle$, since the second term in the right hand side of Eq. (9) is always positive.

The expression for the second term in the right hand side of Eq. (8) is fairly complicated, here we write it in a simpler form by introducing some new parameters, viz., $\gamma := \lambda^2/2D$, $Pe := x_0\lambda/2D$, and $\kappa := \sqrt{1 + [4D(\alpha + \beta)/\lambda^2]} - 1$, such that

$$f := \left. \frac{\partial \langle T_r^G \rangle}{\partial r} \right|_{r=0} = \frac{\beta}{2\gamma^2\alpha} \left[\frac{2Pe - 1}{\kappa} - \frac{2}{\kappa^2(\kappa + 1)} + \frac{2\gamma e^{-\kappa Pe}}{\kappa(\alpha + \beta)} \right] + \frac{1}{2\gamma^2} Pe(Pe - 1). \quad (10)$$

Note that Pe in Eq. (10) is the Péclet number, i.e., the ratio between the rate of driven transport to that of diffusive transport and γ^{-1} is the fastest first-passage time (smallest decay time) in the strong drift limit as was pointed out by Redner in⁶³.

It is evident from Eq. (8) that in the limit $r \rightarrow 0$, resetting is expected to expedite the completion of the process, i.e., $\langle T_r^G \rangle < \langle T^G \rangle$, when $f < 0$. This is a sufficient condition (may not be necessary) for resetting to be useful. When $f > 0$, however, resetting is expected to delay the completion of the process, i.e., $\langle T_r^G \rangle > \langle T^G \rangle$. Therefore, the condition $f = 0$ should divide the entire phase space created by (λ, p_r) in two parts; one where resetting is beneficial ($f < 0$) and the other where it is not ($f > 0$). Indeed, when we plot $f = 0$ following Eq. (10) in the same phase diagram presented in Fig. 5, it exactly overlaps on the existing separatrix plotted earlier by calculating the critical drift λ_c as a function of p_r . Therefore, the condition $f < 0$ marks the phase where introduction of resetting accelerates transport to the target (white regime) while $f > 0$ marks the phase where introduction of resetting delays the same (gray regime), as expected. Revisiting Eq. (10), we note that in the limit of $p_r \rightarrow 1$ (for $\beta \rightarrow 0$),

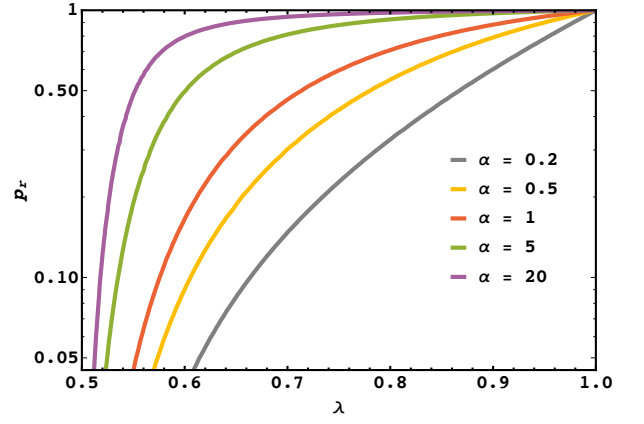


FIG. 6. A phase diagram of p_r vs. λ for different values of α . Each phase boundary (obtained for a certain value of α , shown by the curves) divides the phase space into a “resetting-beneficial” phase (left to the curve) and a “resetting-detrimental” phase (right to the curve). For large values of α , the “resetting-beneficial” phase becomes considerably smaller as the “resetting-detrimental” phase occupies the majority of the phase space.

the first term of Eq. (10) vanishes. Then, $f < 0$ boils down to $Pe < 1$ (meaning $Pe = 1$ is the resetting transition point), the condition where resetting accelerates ungated drift-diffusion, as obtained in earlier works^{50,51,55}.

The phase diagram in Fig. 5 is generated only for a fixed value for α . Next, we perform similar exercise for other values of α and display the results in Fig. 6. It is evident from Fig. 6 that the separatrix, i.e. the phase boundary that separates the two phases – the “resetting-beneficial” phase at the left and the “resetting-detrimental” at the right – varies with α . In fact, for larger values of α , the separatrix divides the phases in such a way that the “resetting-beneficial” phase becomes considerably smaller and the “resetting-detrimental” phase occupies most of the phase space, implying that the effect of resetting becomes rather constrained in that limit. Next, we examine two important limits of the gating rates, viz., $\alpha \rightarrow 0$ and $\alpha, \beta \rightarrow \infty$.

A. The limit $\alpha \rightarrow 0$

The limit $\alpha \rightarrow 0$ essentially implies that the target is reflective almost all the time. In what follows, we will show that this is a delicate limit and should be handled carefully. Strictly speaking, the limit $\alpha \rightarrow 0$ should be interpreted as $\beta \gg \alpha$, which means that the target has higher probability to remain non-reactive than being reactive. Using this limit in Eq. (6), one finds

$$\langle T_r^G \rangle = \frac{1}{r} (e^{\mu_1 x_0} - 1) + \frac{\beta \mu_1}{r \alpha \mu_2} e^{\mu_1 x_0}, \quad (11)$$

where $\mu_1 = (-\lambda + \sqrt{\lambda^2 + 4Dr})/2D > 0$ and $\mu_2 = (-\lambda + \sqrt{\lambda^2 + 4D(\alpha + \beta + r)})/2D > 0$, as before. Moreover, one can disregard the first term in the right hand side of Eq. (11)

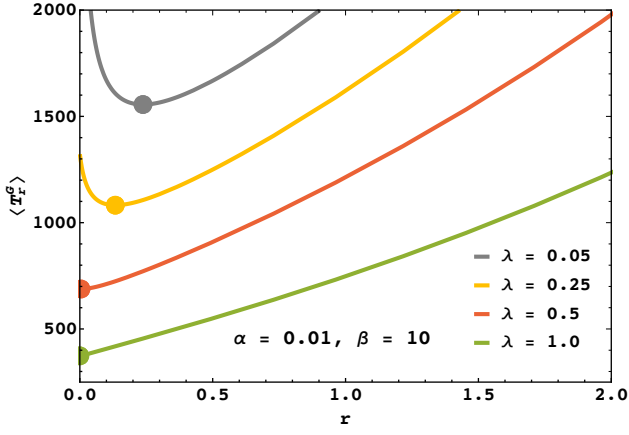


FIG. 7. Monotonic and non-monotonic behaviour of the MFPT in the limit $\alpha \rightarrow 0$ (i.e., $\beta/\alpha \gg 1$), as obtained from Eq. (12). The non-monotonic behaviour gradually vanishes as λ goes beyond the resetting transition point $\lambda_c = D/x_0 = 0.5$. This can be obtained by setting r^* in Eq. (13) to zero.

for finite resetting rate r (assuming $\beta \gg r$) to find

$$\langle T_r^G \rangle = \frac{\beta \left(\sqrt{4Dr + \lambda^2} - \lambda \right) e^{\frac{x_0(\sqrt{4Dr + \lambda^2} - \lambda)}{2D}}}{\alpha r \left(\sqrt{4\beta D + \lambda^2} - \lambda \right)}. \quad (12)$$

To understand the behavior of the average MFPT, we plot $\langle T_r^G \rangle$ as a function of the resetting rate in Fig. 7 for large β and small α keeping $\beta/\alpha \gg 1$. Intriguingly, we find that in this limit, $\langle T_r^G \rangle$ shows both monotonic and non-monotonic behavior as one varies r for different λ . In particular, the latter case implies that there exists a resetting rate for which $\langle T_r^G \rangle$ becomes optimally minimum. To find this optimal resetting rate, we set $\left. \frac{d\langle T_r^G \rangle}{dr} \right|_{r=r^*} = 0$ and obtain

$$r^* = \frac{D}{x_0^2} - \frac{\lambda}{x_0}, \quad (13)$$

which is a simple function of the diffusion constant, initial position and drift. The linear behavior of r^* with respect to the drift variable λ is also noteworthy. Finally, setting $\lambda = 0$, one recovers $r^* = D/x_0^2$ which was obtained in⁴⁸.

The appearance of an ORR in the limit $\alpha \rightarrow 0$ i.e., when the target is poorly reactive (the so-called *cryptic* regime^{20,21}) is counter-intuitive in contrast to the case of $\alpha = 0$ (purely reflective boundary). It can be argued that a diffusing particle usually makes several encounters (also aided by the drift) with the target regardless of the target's state. In the current context, although most of the time the particle may remain unsuccessful to find the target in a reactive state, it can still get absorbed whenever there is an element of chance for the target to become reactive. More details about such cryptic targets and their natural appearances in chemical, biological and ecological systems can be found in^{2,20,52,53}.

B. The limit $\alpha, \beta \rightarrow \infty$

In the limit $\alpha, \beta \rightarrow \infty$, recalling Eq. (10) we can approximate $\kappa \approx \sqrt{4D(\alpha + \beta)}/\lambda$. Thus, one can safely neglect the terms of order $O(\frac{1}{\kappa^2})$ including the exponential term. Under this assumption, setting $f = 0$ in Eq. (10) we obtain an exact expression for the critical drift λ_c that reads

$$\lambda_c = \frac{2D}{x_0} \left[\frac{D + x_0 \frac{\alpha}{\beta} \sqrt{\alpha + \beta} \sqrt{D}}{2D + x_0 \frac{\alpha}{\beta} \sqrt{\alpha + \beta} \sqrt{D}} \right]. \quad (14)$$

We notice that even in this limit p_r does not solely control the dynamics of the system. More from the physical point of view, one can refer to this limit as the partially reactive boundary, where the target switches between the reactive and non-reactive states so fast (i.e., the time scale of such switch is much smaller compared to the time scale of drift-diffusion) that the particle feels an average state of the target and interacts with it with a certain probability all the time – see also^{2,20}.

So far, we performed a detailed analysis to understand the effect of resetting on the dynamics of gated drift-diffusion. In the next section, we turn our attention to the maximal speedup that can be gained by resetting the process at an optimal rate.

IV. THE MAXIMAL SPEEDUP FOR PROCESS COMPLETION

The maximal speedup, i.e., the speedup rendered by optimal resetting rate r^* , is generally defined as the ratio of the MFPT of the original (underlying) process without resetting to that of the process with optimal resetting. Therefore, setting $r = r^*$ in Eq. (6) and utilizing Eq. (9), we obtain the maximal speedup for *gated* drift-diffusion process in a straightforward way, which reads

$$\frac{\langle T^G \rangle}{\langle T_{r^*}^G \rangle} = \begin{cases} \frac{r^*(\alpha + \beta)(2D\beta + x_0\alpha\mu_2^*)}{\lambda \left[r\beta\mu_1^* e^{\frac{x_0}{2D}(\mu_1^* + \mu_2^*)} + (\alpha + \beta) \left[e^{\frac{x_0\mu_1^*}{2D}} (\beta\mu_1^* + \alpha\mu_2^*) - \alpha\mu_2^* \right] \right]} & \text{for } \lambda < \lambda_c \\ 1 & \text{for } \lambda \geq \lambda_c, \end{cases} \quad (15)$$

where $\mu_1^* = \mu_1(r^*)$ and $\mu_2^* = \mu_2(r^*)$, μ_1 and μ_2 having the expressions given after Eq. (6). In Fig. 8, we plot $\langle T^G \rangle / \langle T_{r^*}^G \rangle$ for different values of the reactive occupancy p_r . Fig. 8 indicates that the maximal speedup for gated drift-diffusion is most marked when drift towards the target is negligible. With increase in λ , it gradually decreases to finally become unity at the point of resetting transition, λ_c . We see that when $p_r = 1$, i.e., in the absence of gating, the resetting transition is observed at $\lambda_c = 1$ for our choice of parameters⁵⁰, but when p_r is decreased below unity, the transition is observed for lower values of λ_c , as observed earlier in Fig. 5.

Next, we compare $\langle T_{r^*}^G \rangle$ to $\langle T \rangle$, the MFPT for *ungated* drift-diffusion without resetting, to explore whether it is possible to overcome the increase in the MFPT due to gating by resetting the process in an optimal way. Recalling that the MFPT of ungated drift-diffusion is given by $\langle T \rangle = x_0/\lambda$ and

utilizing Eq. (6) for $r = r^*$ as before, we get

$$\frac{\langle T \rangle}{\langle T_{r^*}^G \rangle} = \begin{cases} \frac{r^* x_0 \alpha (\alpha + \beta) \mu_2^*}{\lambda \left[r \beta \mu_1^* e^{\frac{x_0}{2D} (\mu_1^* + \mu_2^*)} + (\alpha + \beta) \left[e^{\frac{x_0 \mu_1^*}{2D}} (\beta \mu_1^* + \alpha \mu_2^*) - \alpha \mu_2^* \right] \right]} & \text{for } \lambda < \lambda_c \\ \frac{x_0 \alpha \mu_2^*}{2D \beta + x_0 \alpha \mu_2^*} & \text{for } \lambda \geq \lambda_c. \end{cases} \quad (16)$$

Plotting $\langle T \rangle / \langle T_{r^*}^G \rangle$ as a function of λ in Fig. 9 for different values of p_r , we see that the maximal speedup compared to the original ungated process is infinite when there is no drift towards the target and it decreases with an increase in λ , as expected. In fact, Fig. 9 clearly shows that for sufficiently low values of λ , optimal resetting can make the process even > 10 times faster! It proves that resetting is indeed a useful strategy to compensate for the delay due to gating, and when the dynamics is diffusion-controlled, it can even improve the rate of transport (which is inversely proportional to the mean completion time) beyond the original ungated process without resetting. It is also observed from Fig. 9 that in the absence of gating (when $p_r = 1$), the minimal possible value for $\langle T \rangle / \langle T_{r^*}^G \rangle$ is unity, which is achieved for $\lambda \geq \lambda_c$ ⁵⁰. In contrast, when $p_r < 1$, $\langle T \rangle / \langle T_{r^*}^G \rangle$ is reduced below unity even before the resetting transition sets in. Therefore, denoting λ_c^0 as the critical value of λ [marked in Fig. 9 by the colored discs] where $\langle T \rangle / \langle T_{r^*}^G \rangle$ becomes unity for a certain p_r , we observe that $\lambda_c^0 \leq \lambda_c$. The equality holds only for the ungated process and the difference between λ_c^0 and λ_c is prominent for lower values of p_r . These observations lead us to identify all the possible distinct regimes where resetting can benefit the completion of the gated drift-diffusion process. In what follows, we construct a comprehensive phase diagram in the parameter

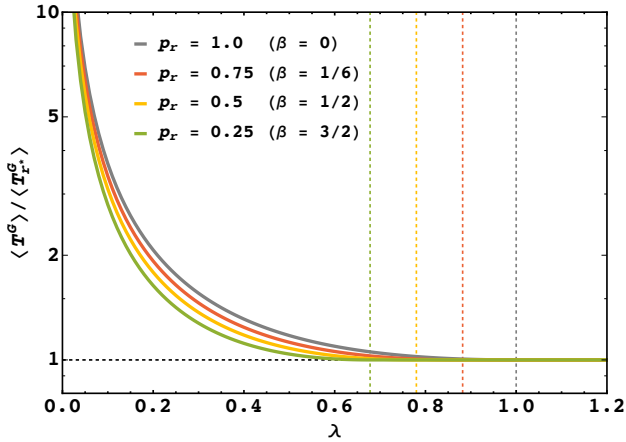


FIG. 8. The maximal speedup for the gated process with resetting compared to the gated process without resetting, $\langle T^G \rangle / \langle T_{r^*}^G \rangle$, vs the drift velocity λ , for different values of the reactive occupancy, p_r . The vertical dashed lines mark the points of resetting transitions for curves of same color, denoted λ_c , such that $\langle T^G \rangle / \langle T_{r^*}^G \rangle > 1$ for $\lambda < \lambda_c$, and $\langle T^G \rangle / \langle T_{r^*}^G \rangle = 1$ at $\lambda \geq \lambda_c$. We take $D = 1$, $x_0 = 2$ and $\alpha = 0.5$ [i.e., $p_r = 1/(2\beta + 1)$] for all cases. In the absence of gating ($p_r = 1$, gray curve), the resetting transition is observed at $\lambda_c = 2D/x_0 = 1$, and λ_c decreases when gating is introduced ($p_r < 1$).

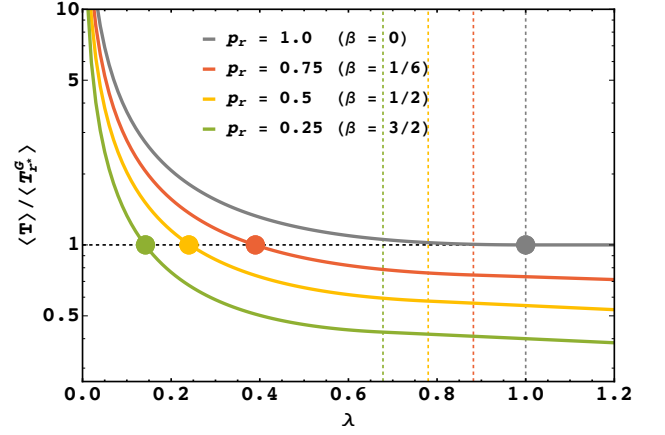


FIG. 9. The maximal speedup for the gated process with resetting compared to the ungated process without resetting, $\langle T \rangle / \langle T_{r^*}^G \rangle$, vs λ , for different values of p_r . The vertical dashed lines mark the points of resetting transition (λ_c) for curves of same color, whereas the colored discs mark the values of λ_c^0 , such that optimal resetting expedites gated process beyond the original ungated process only when $\lambda < \lambda_c^0$. Here $D = 1$, $x_0 = 2$ and $\alpha = 0.5$ [i.e., $p_r = 1/(2\beta + 1)$] for all cases. In the absence of gating ($p_r = 1$, gray curve), the point of resetting transition ($\lambda_c = 2D/x_0 = 1$) coincides with λ_c^0 .

space encapsulating all these effects of resetting.

V. THE COMPLETE PHASE DIAGRAM

To construct the complete phase diagram for the problem, we revisit Fig. 5 and Fig. 8, and recall that the entire phase space [spanned by (λ, p_r)] is divided into two parts, viz., $\langle T_{r^*}^G \rangle < \langle T^G \rangle$ [i.e., where optimal resetting expedites transport] and $\langle T_{r^*}^G \rangle \geq \langle T^G \rangle$ [i.e., where optimal resetting can not expedite transport], and the transition between these two phases takes place at a critical point $\lambda = \lambda_c$. The study of the maximal speedup of the gated process with resetting compared to the ungated process without resetting in Section IV suggests that we can further divide the former phase in two parts: one where the rate of transport for the gated process with optimal resetting is higher than that of original ungated process i.e., $\langle T_{r^*}^G \rangle < \langle T \rangle$ and the other where it is not i.e., $\langle T_{r^*}^G \rangle \geq \langle T \rangle$. The transition between these two phases happens at $\lambda = \lambda_c^0 \leq \lambda_c$. Since gating essentially makes drift-diffusion slower in the absence of resetting, i.e., $\langle T \rangle < \langle T^G \rangle$ [see Eq. (9)], summarizing our observations, we construct a complete phase diagram for the present problem [displayed in Fig. 10], which consists of three distinct phases: (i) phase I: when optimal resetting makes the gated process faster than the original ungated (and hence the original gated) process, given by $\langle T_{r^*}^G \rangle < \langle T \rangle < \langle T^G \rangle$, (ii) phase II: when optimal resetting makes the gated process faster than the original gated process, but not the original ungated process, given by $\langle T \rangle \leq \langle T_{r^*}^G \rangle < \langle T^G \rangle$, and (iii) phase III: when resetting can not make the gated process faster than the original gated (and hence the original ungated) process, given by $\langle T \rangle < \langle T^G \rangle \leq \langle T_{r^*}^G \rangle$. The

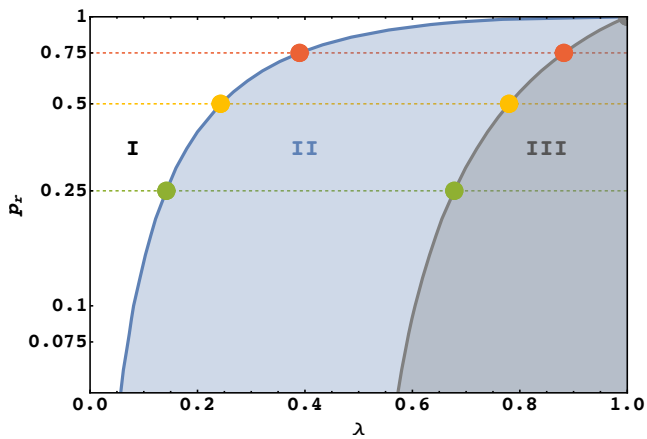


FIG. 10. A complete phase diagram of p_r vs. λ showing three distinct phases; (i) phase I: where optimal resetting enhances the rate of gated drift-diffusion beyond the original (without resetting) ungated process, given by $\langle T_{r^*}^G \rangle < \langle T \rangle < \langle T^G \rangle$, (ii) phase II: when optimal resetting improves the rate of the gated process, but not compared to the original ungated process, given by $\langle T \rangle \leq \langle T_{r^*}^G \rangle < \langle T^G \rangle$, and (iii) phase III: when resetting can not improve the rate of gated process, given by $\langle T \rangle < \langle T^G \rangle \leq \langle T_{r^*}^G \rangle$. The horizontal colored lines mark the cases shown in Fig. 9. Here we consider $\alpha = 0.5$ [such that $p_r = 1/(2\beta + 1)$], $D = 1$ and $x_0 = 2$. Phases I and II merge together at $\lambda_c = 2D/x_0 = 1$, the point of resetting transition for drift-diffusion in the absence of gating ($p_r = 1$).

transition points λ_c^0 create the separatrix between phases I and II, whereas the transition points λ_c create that between phases II and III. Since $\lambda_c^0 = \lambda_c$ for $p_r = 1$, in Fig. 10 we find phases I and II to merge together in the absence of gating. This diagram in the phase space of two important parameters of the system, namely the reactive occupancy and the bias, allows us to delineate the exact nature of resetting in the process completion. In other words, we can gain maximal benefits from a precise and *a priori* knowledge of the parameter space.

VI. CONCLUSIONS

In this work, we performed an in-depth analysis on the completion time statistics of drift-diffusive transport to a stochastically gated target in the presence of Poissonian resetting. In particular, we strategically explored the conditions where resetting can enhance the rate of such transport as has been shown for ungated processes where resetting stabilizes the non-equilibrium motion^{30,45,64–66} by removing the detrimental long trajectories that result in a slower transport rate. Projecting the general problem of gated drift-diffusion with resetting to a gated chemical reaction initiated by a catalyst [as discussed in Fig. 1], the main results of the present work can be interpreted as follows.

We observed that the rate of product formation depends on an interesting interplay between the chemical potential drive that governs the reaction (λ), the probability (p_r) that gated reactant stays in its activated state [when R_2 exists as R_2^*], and

the rate of unbinding (or resetting, with rate r) of the catalyst C from CR_1 . When the chemical potential drive towards the product ($\lambda > 0$) is low/moderate such that the reaction is diffusion-controlled, the rate of reaction is maximized for an optimal unbinding rate (r^*) of the catalyst. In contrast, when the drive λ is strong, i.e., the reaction is drift-controlled, unbinding of the catalyst C from CR_1 decreases the rate of reaction. A transition is thus observed at a critical drive, λ_c , which grows with p_r and becomes maximum for $p_r = 1$, i.e., for the ungated reaction. Strikingly enough, we observed that for $\lambda < \lambda_c^0$ [when $\lambda_c^0 \leq \lambda_c$ is another critical value of λ that increases with p_r and attains a maximum $\lambda_c^0 = \lambda_c$ at $p_r = 1$], optimal unbinding with a rate r^* can make the reaction even > 10 times faster compared to the ungated reaction in the limit $r \rightarrow 0$ (i.e., where the binding step is almost irreversible).

These observations lead to a complete phase diagram based on the *qualitative* and *quantitative* effect of optimal unbinding (resetting) on gated chemical reaction [modeled by drift-diffusion to a gated target] that consists of three distinct phases. Recalling that⁶⁰ rate of product formation \propto (mean completion time of reaction)⁻¹, these three phases are identified through the following conditions: (i) where $\langle T_{r^*}^G \rangle < \langle T \rangle < \langle T^G \rangle$, i.e., where the rate of gated chemical reaction is enhanced by optimal unbinding of catalyst beyond that of ungated/gated reactions when the binding is almost irreversible [$r \rightarrow 0$], (ii) where $\langle T \rangle \leq \langle T_{r^*}^G \rangle < \langle T^G \rangle$, i.e., when optimal unbinding improves the rate of gated reaction, but not beyond the ungated reaction in the limit $r \rightarrow 0$, and (iii) where $\langle T \rangle < \langle T^G \rangle \leq \langle T_{r^*}^G \rangle$, i.e., when unbinding fails to make the gated reaction faster than either of the gated/ungated reaction for almost irreversible binding.

The model considered herein generally applies to gated drift-diffusion under the influence of resetting. The major advantage besides its analytical tractability is that one can also gain deep insights about the intricate trade-offs between gating and resetting mechanisms, both of which are essential components of chemical reaction networks. Generalization of this simple model to a generic space-dependent diffusion process in an arbitrary energy landscape in the presence of gated targets would be a potential research avenue. A detailed numerical analysis to this end would be a worthwhile pursuit. Notably, such theoretical models can capture physical situations arising in experiments that study, e.g., completion time statistics of protein folding by gated fluorescence quenching. There, the protein is tagged/labelled by a fluorophore reversibly binds the protein (here unbinding is similar to resetting) to impart fluorescence properties⁶⁷. Once the tagged protein folds to its native state, the quencher selectively reacts with the active site of that folded protein in its fluorescent state, provided that site is in its open (exposed) conformation. If the active site of the folded protein remains in a closed (hidden) conformation, the quencher fails to react with it, which implicates gating. A successful reaction thus occurs only in the exposed conformation, which leads to subsequent quenching of fluorescence thereby marking the completion of the folding process⁶⁸. We believe that our work can shed light in understanding and harnessing various gating and resetting protocols inherent to such systems.

ACKNOWLEDGEMENT

AP gratefully acknowledges research support from the DST-SERB Start-up Research Grant Number SRG/2022/000080 and the Department of Atomic Energy, Govt. of India. DM thanks SERB (Project No. ECR/2018/002830/CS), DST, Govt. of India, for financial support and IIT Tirupati for the new faculty seed grant. SR acknowledges the Elizabeth Gardner Fellowship by School of Physics & Astronomy, University of Edinburgh and the INSPIRE Faculty research grant by DST, Govt. of India, executed at IIT Tirupati. The numerical calculations reported in this work were carried out on the Nandadevi cluster, which is maintained and supported by IMSc's High-Performance Computing Center. For the purpose of open access, the authors have applied a Creative Commons Attribution (CC BY) licence to any Author Accepted Manuscript version arising from this submission. We thank the anonymous Reviewers for their insightful remarks.

DATA AVAILABILITY

The data that supports the findings of this work are available within the paper, its appendices, and in⁶⁹.

Appendix A: Calculation of the average MFPT by solving Eq. (1) in the Laplace space

Here, we provide the solution of Eq. (1) in the Laplace space. Following that, we calculate the mean first passage time for a diffusing particle with drift, starting from an initial position x_0 , to reach the gated target. We start by Laplace transforming Eq. (1)

$$\begin{aligned} D \frac{\partial^2 \tilde{Q}_0(s|x_0)}{\partial x_0^2} - \lambda \frac{\partial \tilde{Q}_0(s|x_0)}{\partial x_0} - (s + \alpha + r) \tilde{Q}_0(s|x_0) + \alpha \tilde{Q}_1(s|x_0) \\ = -1 - r \tilde{Q}_0(s|x_r) \\ D \frac{\partial^2 \tilde{Q}_1(s|x_0)}{\partial x_0^2} - \lambda \frac{\partial \tilde{Q}_1(s|x_0)}{\partial x_0} - (s + \beta + r) \tilde{Q}_1(s|x_0) + \beta \tilde{Q}_0(s|x_0) \\ = -1 - r \tilde{Q}_1(s|x_r), \end{aligned} \quad (\text{A.1})$$

where $\tilde{Q}_\sigma(s|y) := \int_0^\infty dt e^{-st} Q_\sigma(t|y)$ denote the Laplace transform of $Q_\sigma(t|y)$. Eq. (A.1) is a second order, linear and non-homogeneous differential equation. Considering

$$\tilde{Q}_\sigma(s|x_0) = \tilde{Q}_\sigma^h(s|x_0) + \tilde{Q}_\sigma^{inh}(s|x_0), \quad (\text{A.2})$$

where $\tilde{Q}_\sigma^h(s|x_0)$ and $\tilde{Q}_\sigma^{inh}(s|x_0)$ denote the homogeneous and inhomogeneous parts of $\tilde{Q}_\sigma(s|x_0)$, respectively, we can rewrite Eq. (A.1) in two separate parts. The homogeneous

part reads

$$\begin{aligned} D \frac{\partial^2 \tilde{Q}_0^h(s|x_0)}{\partial x_0^2} - \lambda \frac{\partial \tilde{Q}_0^h(s|x_0)}{\partial x_0} - (s + \alpha + r) \tilde{Q}_0^h(s|x_0) \\ + \alpha \tilde{Q}_1^h(s|x_0) = 0, \\ D \frac{\partial^2 \tilde{Q}_1^h(s|x_0)}{\partial x_0^2} - \lambda \frac{\partial \tilde{Q}_1^h(s|x_0)}{\partial x_0} - (s + \beta + r) \tilde{Q}_1^h(s|x_0) \\ + \beta \tilde{Q}_0^h(s|x_0) = 0. \end{aligned} \quad (\text{A.3})$$

Similarly, the inhomogeneous part reads

$$\begin{aligned} -(s + \alpha + r) \tilde{Q}_0^{inh}(s|x_0) + \alpha \tilde{Q}_1^{inh}(s|x_0) = -1 - r \tilde{Q}_0(s|x_r), \\ -(s + \beta + r) \tilde{Q}_1^{inh}(s|x_0) + \beta \tilde{Q}_0^{inh}(s|x_0) = -1 - r \tilde{Q}_1(s|x_r), \end{aligned} \quad (\text{A.4})$$

which is a set of algebraic equations. Solving Eq. (A.4) we obtain

$$\begin{aligned} \tilde{Q}_0^{inh}(s) = \frac{1}{s+r} \left(1 + \frac{r}{s+r+\alpha+\beta} [\alpha \tilde{Q}_1(s|x_r) \right. \\ \left. + (s+r+\beta) \tilde{Q}_0(s|x_r)] \right), \\ \tilde{Q}_1^{inh}(s) = \frac{1}{s+r} \left(1 + \frac{r}{s+r+\alpha+\beta} [\beta \tilde{Q}_0(s|x_r) \right. \\ \left. + (s+r+\alpha) \tilde{Q}_1(s|x_r)] \right). \end{aligned} \quad (\text{A.5})$$

We note that $\tilde{Q}_\sigma^{inh}(s)$ depends on x_r and not on x_0 . Next, we proceed to solve Eq. (A.3). Noting that x_r does not appear in Eq. (A.3), we simply write $\tilde{Q}_\sigma^h(s|x_0) \equiv \tilde{Q}_\sigma^h$ for notational convenience. Writing Eq. (A.3) in a matrix form, we find

$$\begin{aligned} D \frac{\partial^2}{\partial x_0^2} \begin{pmatrix} \tilde{Q}_0^h \\ \tilde{Q}_1^h \end{pmatrix} - \lambda \frac{\partial}{\partial x_0} \begin{pmatrix} \tilde{Q}_0^h \\ \tilde{Q}_1^h \end{pmatrix} \\ + \begin{pmatrix} -(s+\alpha+r) & \alpha \\ \beta & -(s+\beta+r) \end{pmatrix} \begin{pmatrix} \tilde{Q}_0^h \\ \tilde{Q}_1^h \end{pmatrix} = \mathbf{0}. \end{aligned} \quad (\text{A.6})$$

Taking $\Psi = (\tilde{Q}_0^h \ \tilde{Q}_1^h)^T$, we rewrite Eq. (A.6)

$$\begin{aligned} D \frac{\partial^2}{\partial x_0^2} \Psi - \lambda \frac{\partial}{\partial x_0} \Psi + \mathbf{A} \Psi = \mathbf{0}, \\ \text{where } \mathbf{A} = \begin{pmatrix} -(s+\alpha+r) & \alpha \\ \beta & -(s+\beta+r) \end{pmatrix}. \end{aligned} \quad (\text{A.7})$$

We now choose $\Psi = \Phi e^{mx_0}$ as the trial solution of Eq. (A.7), that generates the characteristic equation $Dm^2 \Phi - \lambda m \Phi + \mathbf{A} \Phi = \mathbf{0}$, which gives

$$\begin{pmatrix} Dm^2 - \lambda m - (s+\alpha+r) & \alpha \\ \beta & Dm^2 - \lambda m - (s+\beta+r) \end{pmatrix} \Phi = \mathbf{0}. \quad (\text{A.8})$$

The roots of Eq. (A.8) can be found as

$$\begin{aligned} m_1 &= \frac{\lambda - \sqrt{\lambda^2 + 4D(s+r)}}{2D}, \\ m_2 &= \frac{\lambda - \sqrt{\lambda^2 + 4D(\alpha + \beta + s+r)}}{2D}, \\ m_3 &= \frac{\lambda + \sqrt{\lambda^2 + 4D(s+r)}}{2D}, \\ m_4 &= \frac{\lambda + \sqrt{\lambda^2 + 4D(\alpha + \beta + s+r)}}{2D}. \end{aligned} \quad (\text{A.9})$$

A close inspection of the above roots reveals that m_1 and m_2 are negative, while m_3 and m_4 are positive (since $D, s, r > 0$). Since $\tilde{Q}_\sigma^h \sim e^{m x_0}$, and $\tilde{Q}_\sigma(s|x_0) = 1/s$ for $x_0 \rightarrow \infty$ (because the survival probability $Q_\sigma(t|x_0)|_{x_0 \rightarrow \infty} = 1$ and its Laplace transform is $1/s$), we select only m_1 and m_2 as the plausible roots.

Letting Φ_1 denote the eigenvector corresponding to m_1 and utilizing Eq. (A.8), we get $\Phi_1 = \begin{pmatrix} 1 \\ 1 \end{pmatrix}$. In a similar manner, the eigenvector corresponding to m_2 is given by $\Phi_2 = \begin{pmatrix} -\alpha/\beta \\ 1 \end{pmatrix}$. The general solution of Eq. (A.7) thus reads $\Psi = c_1 \Phi_1 e^{m_1 x_0} + c_2 \Phi_2 e^{m_2 x_0}$, and subsequently

$$\tilde{Q}_0^h = c_1 e^{m_1 x_0} - \frac{\alpha}{\beta} c_2 e^{m_2 x_0}, \quad (\text{A.10})$$

$$\tilde{Q}_1^h = c_1 e^{m_1 x_0} + c_2 e^{m_2 x_0} \quad (\text{A.11})$$

where c_1 and c_2 are constants to be determined in the following. To this end, we use the boundary condition $\frac{\partial Q_0(t|x_0)}{\partial x_0}|_{x_0=0} = 0$ (equivalently, $\frac{\partial \tilde{Q}_0(s|x_0)}{\partial x_0}|_{x_0=0} = 0$) which results in $\frac{\partial \tilde{Q}_0^h(s|x_0)}{\partial x_0}|_{x_0=0} = 0$, since $\tilde{Q}_\sigma^{ih}(s)$ does not depend on x_0 . Applying this in Eq. (A.10) results in

$$c_2 = \left(\frac{\beta}{\alpha} \right) \frac{c_1 m_1}{m_2}. \quad (\text{A.12})$$

To compute c_1 , we recall the other boundary condition (absorbing) $Q_1(t|0) = 0$ (equivalently, $\tilde{Q}_1(s|0) = 0$). Combining Eq. (A.5) and Eq. (A.11) along with the boundary condition at $x_0 = 0$, we can write

$$\begin{aligned} \tilde{Q}_1(s|0) = c_1 + \left(\frac{\beta}{\alpha} \right) \frac{m_1}{m_2} c_1 + \frac{1}{s+r} \left(\frac{r}{s+r+\alpha+\beta} [\beta \tilde{Q}_0(s|x_r) \right. \\ \left. + (s+r+\alpha) \tilde{Q}_1(s|x_r)] + 1 \right) = 0. \end{aligned} \quad (\text{A.13})$$

Incorporating Eq. (A.12) in Eq. (A.13) and solving for c_1 and hence c_2 finally gives

$$\begin{aligned} c_1 &= - \left[\frac{\alpha m_2}{(\alpha m_2 + \beta m_1)(s+r)} \right] \left(1 + \frac{r}{s+r+\alpha+\beta} [\beta \tilde{Q}_0(s|x_r) \right. \\ &\quad \left. + (s+r+\alpha) \tilde{Q}_1(s|x_r)] \right), \\ c_2 &= - \left[\frac{\beta m_1}{(\alpha m_2 + \beta m_1)(s+r)} \right] \left(1 + \frac{r}{s+r+\alpha+\beta} [\beta \tilde{Q}_0(s|x_r) \right. \\ &\quad \left. + (s+r+\alpha) \tilde{Q}_1(s|x_r)] \right). \end{aligned} \quad (\text{A.14})$$

Plugging in everything together into Eq. (A.2), we find

$$\begin{aligned} \tilde{Q}_0(s|x_0) &= c_1 e^{m_1 x_0} - \frac{m_1}{m_2} c_1 e^{m_2 x_0} + \frac{1}{s+r} \left(1 + \right. \\ &\quad \left. \frac{r}{s+r+\alpha+\beta} [\alpha \tilde{Q}_1(s|x_r) + (s+r+\beta) \tilde{Q}_0(s|x_r)] \right), \\ \tilde{Q}_1(s|x_0) &= c_1 e^{m_1 x_0} + \left(\frac{\beta}{\alpha} \right) \frac{m_1}{m_2} c_1 e^{m_2 x_0} + \frac{1}{s+r} \left(1 + \right. \\ &\quad \left. \frac{r}{s+r+\alpha+\beta} [\beta \tilde{Q}_0(s|x_r) + (s+r+\alpha) \tilde{Q}_1(s|x_r)] \right), \end{aligned} \quad (\text{A.15})$$

which are written in terms of $\tilde{Q}_\sigma(s|x_r)$. Setting $x_r = x_0$ in Eq. (A.15) in a self-consistent manner, we find the exact expressions for the survival functions

$$\begin{aligned} \tilde{Q}_0(s|x_0) &= \frac{(\beta m_1 + \alpha m_2) + m_1 e^{m_2 x_0} \left(\alpha + \frac{r(\alpha+\beta)}{\alpha+\beta+s} \right) - \alpha m_2 e^{m_1 x_0}}{\frac{\beta m_1 r s e^{m_2 x_0}}{\alpha+\beta+s} + (\alpha m_2 r e^{m_1 x_0} + \beta m_1 s + \alpha m_2 s)}, \\ \tilde{Q}_1(s|x_0) &= \frac{(\alpha + \beta + s)(\alpha m_2 (e^{m_1 x_0} - 1) + \beta m_1 (e^{m_2 x_0} - 1))}{(\alpha + \beta + s)(\alpha m_2 r e^{m_1 x_0} + \beta m_1 s + \alpha m_2 s) + \beta m_1 r s e^{m_2 x_0}}. \end{aligned} \quad (\text{A.16})$$

The averaged survival probability can be found by substituting Eq. (A.16) into Eq. (3). This results in

$$\tilde{Q}_r^G(s|x_0) = \frac{\beta m_1 \left(\frac{r e^{m_2 x_0}}{\alpha+\beta+s} + 1 \right) + \alpha m_2 (1 - e^{m_1 x_0})}{\frac{\beta m_1 r s e^{m_2 x_0}}{\alpha+\beta+s} + (\alpha m_2 r e^{m_1 x_0} + \beta m_1 s + \alpha m_2 s)}. \quad (\text{A.17})$$

Generically, Eq. (A.17) can be used to derive all the first passage time moments. The observable of our interest in this problem, for example, the averaged MFPT reads $\langle T_r^G \rangle = \tilde{Q}_r^G(s|x_0)|_{s=0}$ ⁶². This results in Eq. (6) in the main text.

Alternatively, we can get Eq. (6) from Eq. (A.15) by calculating individual mean first passage times conditioned on the initial state of the target state. To this end, let us denote $T_\sigma^G(x_0)$ as the first-passage time to reach the target at the origin starting from the position x_0 with initial target state being at σ . Using $\langle T_\sigma^G(x_0) \rangle = \tilde{Q}_\sigma(s|x_0)|_{s=0}$ and setting $s \rightarrow 0$ in Eq. (A.15), we get

$$\begin{aligned} \langle T_1^G(x_0) \rangle &= \frac{1}{r} (e^{\mu_1 x_0} - 1) + \frac{1}{r} \left[\frac{\beta \mu_1}{\alpha \mu_2} e^{\mu_1 x_0} (1 - e^{-\mu_2 x_0}) \right], \\ \langle T_0^G(x_0) \rangle &= \frac{1}{r} (e^{\mu_1 x_0} - 1) \\ &\quad + \frac{1}{r} \left[\frac{\mu_1}{\mu_2} e^{\mu_1 x_0} \left(e^{-\mu_2 x_0} \left(1 + \frac{r}{\alpha} \right) + \frac{\beta}{\alpha} \right) \right], \end{aligned} \quad (\text{A.18})$$

where $\mu_1 := -m_1|_{s=0} > 0$ and $\mu_2 := -m_2|_{s=0} > 0$. Finally, plugging in Eq. (A.18) into Eq. (4) in the main text, we obtain Eq. (6).

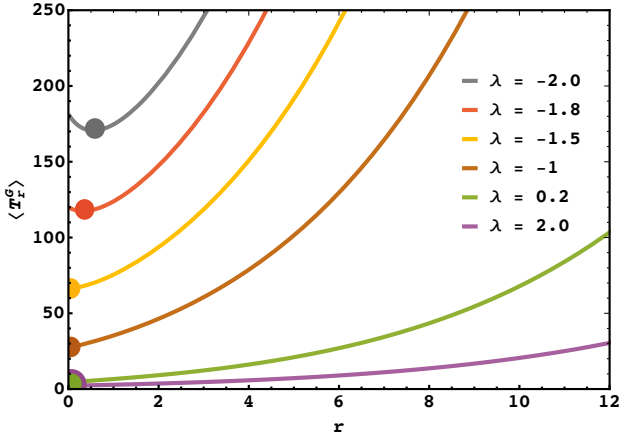


FIG. 11. The average MFPT $\langle T_r^G \rangle$ as a function of the resetting rate r for different values of λ in the case of bounded domain. Here, the reflecting boundary is placed at $L = 3$, where the resetting/initial location is at $x_0 = 2$. The colored discs mark the optimal resetting rate (r^*) in each case. Notably, resetting may not always be helpful ($r^* = 0$) even when $\lambda < 0$ (e.g., yellow and brown curves).

Appendix B: The case of confined geometry

Here we consider the case of a bounded system, i.e., where the particle remains in a finite confinement. This is also highly relevant from the context of chemical reactions, since a high energy barrier can mimic a reflecting boundary (in the reaction coordinate space) that pushes the particle away from it. We construct this finite domain by considering the same setup as in the main text, with an additional reflecting wall at $x = L > x_0$. If the particle hits the wall it gets reflected back. Intuitively, the barrier or the reflecting boundary prevents the particle from going too far from the target placed at the origin. This is in sharp contrast to the semi-infinite case, where the particle is allowed to diffuse away from the target. This leads to a few key changes in the dynamics that are reflected in the average MFPT.

On the technical ground, we can find the survival probability in Laplace space using the same method as discussed in Appendix A with the new boundary condition $\frac{\partial \tilde{Q}_\sigma(t|x_0)}{\partial x_0}|_{x_0=L} = 0$. For this reason, all the eigenvalues will exist unlike in the previous case. In particular, one can show that the eigenvector corresponding to m_3 is the same as m_1 , i.e., $\Phi_1 = \begin{pmatrix} 1 \\ 1 \end{pmatrix}$ and that of m_4 is same as m_2 i.e. $\Phi_2 = \begin{pmatrix} -\alpha/\beta \\ 1 \end{pmatrix}$. Recalling the decomposition $\tilde{Q}_\sigma(s) = \tilde{Q}_\sigma^h(s) + \tilde{Q}_\sigma^{inh}(s)$ from Eq. (A.2), we first try to obtain the solutions for the homogeneous part. As before taking $\Psi = (\tilde{Q}_0^h \quad \tilde{Q}_1^h)^T$ and using Eq. (A.7) we find

$$\Psi = c_1 \Phi_1 e^{m_1 x_0} + c_2 \Phi_2 e^{m_2 x_0} + c_3 \Phi_1 e^{m_3 x_0} + c_4 \Phi_2 e^{m_4 x_0}, \quad (\text{B.1})$$

so that

$$\tilde{Q}_0^h = c_1 e^{m_1 x_0} - \frac{\alpha}{\beta} c_2 e^{m_2 x_0} + c_3 e^{m_3 x_0} - \frac{\alpha}{\beta} c_4 e^{m_4 x_0}, \quad (\text{B.2})$$

$$\tilde{Q}_1^h = c_1 e^{m_1 x_0} + c_2 e^{m_2 x_0} + c_3 e^{m_3 x_0} + c_4 e^{m_4 x_0}. \quad (\text{B.3})$$

The inhomogeneous part $\tilde{Q}_\sigma^{inh}(s)$ has the same solution as given in Eq. (A.5). In addition to the boundary conditions $\tilde{Q}_1(s|0) = 0$ and $\frac{\partial \tilde{Q}_0^h(s|x_0)}{\partial x_0}|_{x_0=0} = 0$ at the gated target, we also have two additional boundary conditions namely $\frac{\partial \tilde{Q}_0(s|x_0)}{\partial x_0}|_{x_0=L} = 0$ and $\frac{\partial \tilde{Q}_1(s|x_0)}{\partial x_0}|_{x_0=L} = 0$. These four boundary conditions give four linear equations

$$\begin{aligned} c_1 + c_2 + c_3 + c_4 + \tilde{Q}_1^{inh}(s) &= 0, \\ c_1 m_1 e^{m_1 L} + c_2 m_2 e^{m_2 L} + c_3 m_3 e^{m_3 L} + c_4 m_4 e^{m_4 L} &= 0, \\ c_1 m_1 e^{m_1 L} - \frac{\alpha}{\beta} c_2 m_2 e^{m_2 L} + c_3 m_3 e^{m_3 L} - \frac{\alpha}{\beta} c_4 m_4 e^{m_4 L} &= 0, \\ c_1 m_1 - \frac{\alpha}{\beta} c_2 m_2 + c_3 m_3 - \frac{\alpha}{\beta} c_4 m_4 &= 0, \end{aligned} \quad (\text{B.4})$$

which completely determine the constants c_1, c_2, c_3, c_4 . From this, we can find a closed-form expression for the survival probabilities in Laplace space (and subsequently the MFPT by setting $s \rightarrow 0$). The expression for the MFPT is quite lengthy to present here; check⁶⁹ for the *Mathematica* file where all the derivations are given. In what follows, we perform a comprehensive analysis of this MFPT and point out the key differences in comparison to the that obtained for the semi-infinite domain.

Fig. 11 showcases the variation of the MFPT, $\langle T_r^G \rangle$, as a function of the resetting rate r for different values of the drift λ . One crucial observation is that the non-monotonic behaviour of $\langle T_r^G \rangle$ is *not always present* even when the drift is away from the target (i.e., $\lambda < 0$). This is in complete contrast to the semi-infinite case where resetting is guaranteed to help whenever the drift is away from the target [see Fig. (3)]. To understand this better, we plot the optimal resetting rate r^* as a function of λ for various domain sizes L in Fig. 12, which clearly shows that the critical values of λ that marks the resetting transition (denoted λ_c in the main text; the minimal value of λ for which $r^* = 0$), can be negative for considerably smaller domains. With increasing L , however, λ_c starts to increase and for sufficiently large values of L it saturates to the value of λ_c for the semi-infinite case, as displayed Fig. 5 of the main text. Simply put, if the reflecting boundary starts moving sufficiently away from the target, the MFPT starts to increase and resetting renders a more effective search in that case.

To elaborate this further, one can expand the MFPT (for finite domain) in the limit of small resetting rate $r \rightarrow 0$ and find the first order correction in r [in similar spirit as in Eq. (8) – see the discussion for the semi-infinite case in Sec. III, particularly around Eq. (10)]. The arguments on the function f as discussed there still holds for the present case (of course, the exact form of the function will be different here). Thus, setting $f = 0$ gives us the separatrix distinguishing between the region where resetting helps ($f < 0$) and where it hinders ($f > 0$). Utilizing this fact, we generate a phase diagram by plotting λ_c as a function of L , the distance between the reflecting barrier and the origin, and present the same in the inset of Fig. 12. The semi-infinite limit is obtained by taking $L \rightarrow \infty$, where λ_c saturates to the corresponding value calculated/presented in the main text. For example, we see from

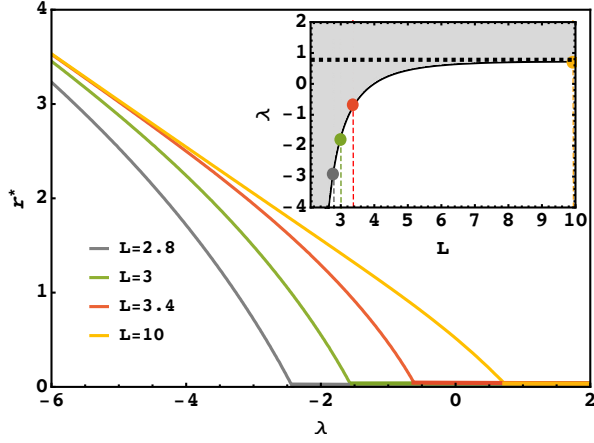


FIG. 12. Main: Variation of ORR (r^*) as a function of λ for different domain size L . For $\lambda < \lambda_c$, resetting proves itself beneficial, as indicated by the non-zero values of r^* , whereas for $\lambda \geq \lambda_c$, resetting becomes detrimental, as indicated by $r^* = 0$. The resetting transition is thus marked by λ_c . Inset: Phase diagram with reflecting barrier at L , by plotting λ_c that acts as the separatrix (black line; the colored discs mark the specific cases shown in the main panel) that divides the phase space in two parts; one where resetting is beneficial (white regime) and the other where resetting is detrimental (gray regime). Existence of negative λ_c essentially implies that resetting can be detrimental even when $\lambda < 0$. The dashed horizontal line corresponds to $\lambda_c = 0.78$, obtained for the semi-infinite case (i.e. $L \rightarrow \infty$), as displayed in Fig. 5 for $p_r = 0.5$. Note that we consider $\alpha = 0.5$, $\beta = 0.5$ and $D = 1$ for each case in the main panel and in the inset.

Fig. 12 that when $p_r = 0.5$, λ_c saturates to 0.78, the critical value of λ for $p_r = 0.5$ (marked in Fig. 5 by the vertical yellow line).

Appendix C: The average MFPT for gated drift-diffusion without resetting

In the absence of resetting, the backward master equations in terms of the survival probability read

$$\begin{aligned} \frac{\partial Q_0^{r=0}(t|x_0)}{\partial t} &= -\lambda \frac{\partial Q_0^{r=0}(t|x_0)}{\partial x_0} + D \frac{\partial^2 Q_0^{r=0}(t|x_0)}{\partial x_0^2} \\ &\quad + \alpha [Q_1^{r=0}(t|x_0) - Q_0^{r=0}(t|x_0)] \\ \frac{\partial Q_1^{r=0}(t|x_0)}{\partial t} &= -\lambda \frac{\partial Q_1^{r=0}(t|x_0)}{\partial x_0} + D \frac{\partial^2 Q_1^{r=0}(t|x_0)}{\partial x_0^2} \\ &\quad + \beta [Q_0^{r=0}(t|x_0) - Q_1^{r=0}(t|x_0)]. \end{aligned} \quad (\text{C.1})$$

Solving Eq. (C.1), we obtain the following expressions for the survival functions in the Laplace space

$$\begin{aligned} \tilde{Q}_0^{r=0}(s|x_0) &= \frac{1}{s} - \frac{1}{s} \frac{\alpha n_2}{\beta n_1 + \alpha n_2} \left(e^{-n_1 x_0} - \frac{n_1 e^{-n_2 x_0}}{n_2} \right), \\ \tilde{Q}_1^{r=0}(s|x_0) &= \frac{1}{s} - \frac{1}{s} \frac{\alpha n_2}{\beta n_1 + \alpha n_2} \left(e^{-n_1 x_0} + \frac{\beta n_1 e^{-n_2 x_0}}{\alpha n_2} \right), \end{aligned} \quad (\text{C.2})$$

where $n_1 = \frac{-\lambda + \sqrt{4Ds + \lambda^2}}{2D}$ and $n_2 = \frac{-\lambda + \sqrt{4D(\alpha + \beta + s) + \lambda^2}}{2D}$. Setting $s \rightarrow 0$, the underlying MFPTs can be computed as before. Eventually, one finds

$$\langle T_0^{r=0} \rangle = \frac{x_0}{\lambda} + \frac{2D \left(\beta + \alpha e^{-\frac{x_0 (\sqrt{4D(\alpha + \beta) + \lambda^2} - \lambda)}{2D}} \right)}{\alpha \lambda \left(-\lambda + \sqrt{4D(\alpha + \beta) + \lambda^2} \right)}, \quad (\text{C.3})$$

$$\langle T_1^{r=0} \rangle = \frac{x_0}{\lambda} + \frac{2\beta D \left(-e^{-\frac{x_0 (\sqrt{4D(\alpha + \beta) + \lambda^2} - \lambda)}{2D}} + 1 \right)}{\alpha \lambda \left(-\lambda + \sqrt{4D(\alpha + \beta) + \lambda^2} \right)}. \quad (\text{C.4})$$

The averaged MFPT is then given by

$$\begin{aligned} \langle T^G \rangle &= p_r \langle T_1^{r=0} \rangle + (1 - p_r) \langle T_0^{r=0} \rangle \\ &= \frac{x_0}{\lambda} + \frac{2\beta D}{\alpha \lambda \left(\sqrt{4D(\alpha + \beta) + \lambda^2} - \lambda \right)}. \end{aligned} \quad (\text{C.5})$$

Note that for $p_r \rightarrow 1$ ($\beta \rightarrow 0$), Eq. (C.5) reduces to $\langle T \rangle = x_0/\lambda$, as expected. Moreover, since $D, \alpha, \beta > 0$, the second term of the expression of $\langle T^G \rangle$ in Eq. (C.5) is always positive, which clearly shows $\langle T^G \rangle > \langle T \rangle$.

Appendix D: Details of numerical simulations

In this Appendix, we sketch out the basic steps used for the numerical simulations in the main text. We recall that the particle starts from and resets to x_0 at a rate r . In between reset events, it diffuses in the presence of a drift λ . Evolution of this particle in microscopic time scale Δt can be written in the form of a Langevin dynamics such as

$$x(t + \Delta t) = \begin{cases} x_0 & \text{w.p. } r\Delta t \\ x(t) - \lambda \Delta t + \sqrt{2D\Delta t} \eta(t) & \text{w.p. } (1 - r\Delta t) \end{cases} \quad (\text{D.1})$$

where $\eta(t)$ is a δ -correlated white noise i.e., a Gaussian random variable with zero mean and unit variance. Note that the abbreviation w.p. in Eq. (D.1) has full-form *with probability*. We evolve the particle at each time step Δt in our simulation according to Eq. (D.1) until the particle reaches the target at $x = 0$. However, to implement the gating condition to the target, we define a state variable $\sigma = (0, 1)$ representing the non-reactive and reactive states of the target, respectively. If target is initially at the non-reactive state, it switches to the reactive state with probability $\alpha \Delta t$. Similarly, it is switched from the active state to the inactive one with probability $\beta \Delta t$.

To compute the first passage time, we simultaneously track two events: (i) the instant when the particle crosses the origin to the negative side i.e., $x \leq 0$ and (ii) note whether the target is in active state i.e., $\sigma = 1$. If both the conditions are satisfied, the particle gets absorbed and the process ends. We measure the corresponding time and put it into the first passage statistics. However, if $x \leq 0$ and $\sigma = 0$ then the particle

gets reflected from the boundary, and the process continues till the next absorption occurs. The reflecting boundary condition is implemented by simply reversing the position of the particle i.e. $x \rightarrow -x$. The initial target state σ is chosen from the steady state i.e.,

$$\sigma(t=0) = \begin{cases} 1 & \text{with probability } p_r, \\ 0 & \text{with probability } (1-p_r), \end{cases} \quad (\text{D.2})$$

where $p_r = \alpha/(\alpha + \beta)$. In our simulations, $\Delta t = 10^{-5}$ and the averaging was done for 10^5 successful trajectories for each value of λ . The results are displayed in Fig. 3 with the star symbols, which show excellent agreement with the analytical results presented by the solid lines of same color.

REFERENCES:

- ¹Maffeo, C., Bhattacharya, S., Yoo, J., Wells D., and Aksimentiev, A., 2012. Modeling and Simulation of Ion Channels, *Chemical Reviews*, 112, p.6250-6284.
- ²Bressloff, P.C., 2014. *Stochastic processes in cell biology* (Vol. 41, pp. 10-1007). Berlin: Springer.
- ³Bressloff, P.C., 2016. Diffusion in cells with stochastically gated gap junctions. *SIAM Journal on Applied Mathematics*, 76(4), pp.1658-1682.
- ⁴Szabo, A., Shoup, D., Northrup, S.H. and McCammon, J.A., 1982. Stochastically gated diffusion-influenced reactions. *The Journal of Chemical Physics*, 77(9), pp.4484-4493.
- ⁵Northrup, S.H., Zarrin, F. and McCammon, J.A., 1982. Rate theory for gated diffusion-influenced ligand binding to proteins. *The Journal of Physical Chemistry*, 86(13), pp.2314-2321.
- ⁶Zhou, H.X. and Szabo, A., 1996. Theory and simulation of stochastically-gated diffusion-influenced reactions. *The Journal of Physical Chemistry*, 100(7), pp.2597-2604.
- ⁷Makhnovskii, Y.A., Berezhkovskii, A.M., Sheu, S.Y., Yang, D.Y., Kuo, J. and Lin, S.H., 1998. Stochastic gating influence on the kinetics of diffusion-limited reactions. *The Journal of chemical physics*, 108(3), pp.971-983.
- ⁸Shin, J. and Kolomeisky, A.B., 2018. Molecular search with conformational change: One-dimensional discrete-state stochastic model. *The Journal of chemical physics*, 149(17), p.174104.
- ⁹Godec, A. and Metzler, R., 2017. First passage time statistics for two-channel diffusion. *Journal of Physics A: Mathematical and Theoretical*, 50(8), p.084001.
- ¹⁰Spouge, J.L., Szabo, A. and Weiss, G.H., 1996. Single-particle survival in gated trapping. *Physical Review E*, 54(3), p.2248.
- ¹¹Gopich, I.V. and Szabo, A., 2016. Reversible stochastically gated diffusion-influenced reactions. *The Journal of Physical Chemistry B*, 120(33), pp.8080-8089.
- ¹²Berezhkovskii, A.M., Yang, D.Y., Lin, S.H., Makhnovskii, Y.A. and Sheu, S.Y., 1997. Smoluchowski-type theory of stochastically gated diffusion-influenced reactions. *The Journal of chemical physics*, 106(17), pp.6985-6998.
- ¹³McCammon, J.A. and Northrup, S.H., 1981. Gated binding of ligands to proteins. *Nature*, 293(5830), pp.316-317.
- ¹⁴Boehr, D.D., Nussinov, R. and Wright, P.E., 2009. The role of dynamic conformational ensembles in biomolecular recognition. *Nature chemical biology*, 5(11), pp.789-796.
- ¹⁵Reingruber, J. and Holcman, D., 2009. Gated narrow escape time for molecular signaling. *Physical review letters*, 103(14), p.148102.
- ¹⁶Szabo, A., Schulten, K. and Schulten, Z., 1980. First passage time approach to diffusion controlled reactions. *The Journal of chemical physics*, 72(8), pp.4350-4357.
- ¹⁷Kochugaeva, M.P., Shvets, A.A. and Kolomeisky, A.B., 2016. How conformational dynamics influences the protein search for targets on DNA. *Journal of Physics A: Mathematical and Theoretical*, 49(44), p.444004.
- ¹⁸Mercado-Vásquez, G. and Boyer, D., 2021. First hitting times between a run-and-tumble particle and a stochastically gated target. *Physical Review E*, 103(4), p.042139.
- ¹⁹Lawley, S.D. and Keener, J.P., 2015. A new derivation of Robin boundary conditions through homogenization of a stochastically switching boundary. *SIAM Journal on Applied Dynamical Systems*, 14(4), pp.1845-1867.
- ²⁰Mercado-Vásquez, G. and Boyer, D., 2019. First hitting times to intermittent targets. *Physical Review Letters*, 123(25), p.250603.
- ²¹Scher, Y. and Reuveni, S., 2021. Unified Approach to Gated Reactions on Networks. *Physical Review Letters*, 127(1), p.018301.
- ²²Scher, Y. and Reuveni, S., 2021. Gated reactions in discrete time and space. *The Journal of Chemical Physics*, 155(23), p.234112.
- ²³Kumar, A., Zodage, A. and Santhanam, M.S., 2021. First detection of threshold crossing events under intermittent sensing. *Physical Review E*, 104(5), p.L052103.
- ²⁴Kumar, A., Scher, Y., Reuveni, S. and Santhanam, M.S., 2022. Inference in gated first-passage processes. arXiv preprint [arXiv:2210.00678](https://arxiv.org/abs/2210.00678).
- ²⁵Reuveni, S., Urbakh, M. and Klafter, J., 2014. Role of substrate unbinding in Michaelis-Menten enzymatic reactions. *Proceedings of the National Academy of Sciences*, 111(12), pp.4391-4396.
- ²⁶Pal, A. and Prasad, V.V., 2019. Landau-like expansion for phase transitions in stochastic resetting. *Physical Review Research*, 1(3), p.032001.
- ²⁷Roldán, É., Lisica, A., Sánchez-Taltavull, D. and Grill, S.W., 2016. Stochastic resetting in backtrack recovery by RNA polymerases. *Physical Review E*, 93(6), p.062411.
- ²⁸Budnar, S., Husain, K.B., Gomez, G.A., Naghibosadat, M., Varma, A., Verma, S., Hamilton, N.A., Morris, R.G. and Yap, A.S., 2019. Anillin promotes cell contractility by cyclic resetting of RhoA residence kinetics. *Developmental cell*, 49(6), pp.894-906.
- ²⁹Yuste, S.B., Abad, E. and Lindenberg, K., 2010. Reaction-subdiffusion model of morphogen gradient formation. *Physical Review E*, 82(6), p.061123.
- ³⁰Evans, M.R. and Majumdar, S.N., 2011. Diffusion with stochastic resetting. *Physical review letters*, 106(16), p.160601.
- ³¹Pal, A., Kundu, A. and Evans, M.R., 2016. Diffusion under time-dependent resetting. *Journal of Physics A: Mathematical and Theoretical*, 49(22), p.225001.
- ³²Ahmad, S., Nayak, I., Bansal, A., Nandi, A. and Das, D., 2019. First passage of a particle in a potential under stochastic resetting: A vanishing transition of optimal resetting rate. *Physical Review E*, 99(2), p.022130.
- ³³Singh, R.K., Metzler, R. and Sandev, T., 2020. Resetting dynamics in a confining potential. *Journal of Physics A: Mathematical and Theoretical*, 53(50), p.505003.
- ³⁴Pal, A. and Prasad, V.V., 2019. First passage under stochastic resetting in an interval. *Physical Review E*, 99(3), p.032123.
- ³⁵Ray, S. and Reuveni, S., 2020. Diffusion with resetting in a logarithmic potential. *The Journal of chemical physics*, 152(23), p.234110.
- ³⁶Ray, S. and Reuveni, S., 2021. Resetting transition is governed by an interplay between thermal and potential energy. *The Journal of Chemical Physics*, 154(17), p.171103.
- ³⁷Ray, S., 2020. Space-dependent diffusion with stochastic resetting: A first-passage study. *The Journal of Chemical Physics*, 153(23), p.234904.
- ³⁸Ali, S. Y., Choudhury, N., and Mondal, D., 2022. Asymmetric restart in a stochastic climate model: A theoretical perspective to prevent the abnormal precipitation accumulation caused by global warming. *Journal of Physics A: Mathematical and Theoretical*, 55, p.301001 (2022).
- ³⁹Ray, S., 2022. Expediting Feller process with stochastic resetting. *Physical Review E*, 106 (3), p.034133.
- ⁴⁰Bonomo, O.L. and Pal, A., 2021. First passage under restart for discrete space and time: application to one-dimensional confined lattice random walks. *Physical Review E*, 103(5), p.052129.
- ⁴¹Bressloff, P. C., 2020, Modeling active cellular transport as a directed search process with stochastic resetting and delays, *J. Phys. A* 53 pp. 355001.
- ⁴²Pal, A. and Reuveni, S., 2017. First passage under restart. *Physical review letters*, 118(3), p.030603.
- ⁴³A. Chechkin and I. M. Sokolov, 2018. Random Search with Resetting: A Unified Renewal Approach, *Phys. Rev. Lett.* 121, p.050601.
- ⁴⁴Kumar, A. and Pal, A., 2023. Universal framework for record ages under restart. *Phys. Rev. Lett.* 130, p.157101.

- ⁴⁵Evans, M.R., Majumdar, S.N. and Schehr, G., 2020. Stochastic resetting and applications. *Journal of Physics A: Mathematical and Theoretical*, 53(19), p.193001.
- ⁴⁶Tal-Friedman, O., Pal, A., Sekhon, A., Reuveni, S. and Roichman, Y., 2020. Experimental realization of diffusion with stochastic resetting. *J. Phys. Chem. Lett.* 2020, 11, 17, 7350–7355
- ⁴⁷Besga, B., Bovon, A., Petrosyan, A., Majumdar, S.N. and Ciliberto, S., 2020. Optimal mean first-passage time for a Brownian searcher subjected to resetting: experimental and theoretical results. *Physical Review Research*, 2(3), p.032029.
- ⁴⁸Mercado-Vásquez, G. and Boyer, D., 2021. Search of stochastically gated targets with diffusive particles under resetting. *Journal of Physics A: Mathematical and Theoretical*, 54(44), p.444002.
- ⁴⁹Bressloff, P.C., 2020. Diffusive search for a stochastically-gated target with resetting. *Journal of Physics A: Mathematical and Theoretical*, 53(42), p.425001.
- ⁵⁰Ray, S., Mondal, D. and Reuveni, S., 2019. Péclet number governs transition to acceleratory restart in drift-diffusion. *Journal of Physics A: Mathematical and Theoretical*, 52(25), p.255002.
- ⁵¹Pal, A., Eliazar, I. and Reuveni, S., 2019. First passage under restart with branching. *Physical review letters*, 122(2), p.020602.
- ⁵²Golding, I., Paulsson, J., Zawilski, S.M. and Cox, E.C., 2005. Real-time kinetics of gene activity in individual bacteria. *Cell*, 123(6), pp.1025-1036.
- ⁵³Gendron, R.P. and Staddon, J.E., 1983. Searching for cryptic prey: the effect of search rate. *The American Naturalist*, 121(2), pp.172-186.
- ⁵⁴Jain, S., Boyer, D., Pal, A. and Dagdug, L., 2023. Fick–Jacobs description and first passage dynamics for diffusion in a channel under stochastic resetting. *The Journal of Chemical Physics*, 158(5), p.054113.
- ⁵⁵Pal, A., Chatterjee, R., Reuveni, S. and Kundu, A., 2019. Local time of diffusion with stochastic resetting. *Journal of Physics A: Mathematical and Theoretical*, 52(26), p.264002.
- ⁵⁶Pal, A., Kostinski, S. and Reuveni, S., 2022. The inspection paradox in stochastic resetting. *Journal of Physics A: Mathematical and Theoretical*, 55(2), p.021001.
- ⁵⁷Reuveni, S., 2016. Optimal stochastic restart renders fluctuations in first passage times universal. *Physical review letters*, 116(17), p.170601.
- ⁵⁸Moffitt, J.R., Chemla, Y.R. and Bustamante, C., 2010. Methods in statistical kinetics. In *Methods in enzymology* (Vol. 475, pp. 221-257). Academic Press.
- ⁵⁹Henzler-Wildman, K. and Kern, D., 2007. Dynamic personalities of proteins. *Nature*, 450(7172), pp.964-972.
- ⁶⁰Makarov, D.E., 2015. *Single molecule science: physical principles and models*. CRC Press.
- ⁶¹Van Kampen, N.G., 1992. *Stochastic processes in physics and chemistry* (Vol. 1). Elsevier.
- ⁶²Gardiner, C.W., 1985. *Handbook of stochastic methods* (Vol. 3, pp. 2-20). Berlin: Springer.
- ⁶³Redner, S., 2001. *A guide to first-passage processes*. Cambridge University Press.
- ⁶⁴Pal, A., 2015. Diffusion in a potential landscape with stochastic resetting. *Physical Review E*, 91(1), p.012113.
- ⁶⁵Eule, S. and Metzger, J.J., 2016. Non-equilibrium steady states of stochastic processes with intermittent resetting. *New Journal of Physics*, 18(3), p.033006.
- ⁶⁶Gupta, D., Plata, C.A. and Pal, A., 2020. Work fluctuations and Jarzynski equality in stochastic resetting. *Physical review letters*, 124(11), p.110608.
- ⁶⁷Zhuang, X., Ha, T., Kim, H. D., Centner T., Labeit, S., and Chu, S., 2000. Fluorescence quenching: A tool for single-molecule protein-folding study. *Proceedings of the National Academy of Sciences*, 97(26), p.14241–14244.
- ⁶⁸Somogyi, B., Norman, J. A., and Rosenberg, A., 1986. Gated quenching of intrinsic fluorescence and phosphorescence of globular protein: An extended model. *Biophysical Journal*, 50, p.55–61.
- ⁶⁹See the [Github link](#) which contains the Mathematica notebook with all the detailed calculations for the confined geometry.